SLAC-PUB-5180
May 1990
(E)

Tau-Charm Factory Design*

B. Barish, R. Stroynowski, A. Weinstein
California Institute of Technology, Pasadena, CA 91125

J.J. Gomez-Cadenas, C. A. Heusch, W. Lockman, A. Seiden
University of California at Santa Cruz, Santa Cruz, CA 95064

R. Johnson, B. Meadows, M. Nussbaum, M. Sokoloff, I. Stockdale
University of Cincinnati, Cincinnati, OH 45221

J. Kirkby
CERN, CH-1211, Geneva 23, Switzerland

B. Eisenstein, G. Gladding, J. Izen, J. Thaler
University of Illinois at Urbana-Champaign, Urbana, IL 61801

R. Cowan, M. Fero, R. Yamamoto
Massachusetts Institute of Technology, Cambridge, MA 02139

J. Brau, R. Frey
University of Oregon, Eugene, OR 97403

M. Allen, T. Barklow, R. Bell, K. Brown, K. Bunnell, D. Coward
D. Faust, D. Fryberger, K.K. Gan, R. Gearhart, T. Jenkins, A. Lisin,
G. Loew, R. Miller, P. Morton, C. Munger, A. Odian,
J. M. Paterson, M. Perl, R. Ruth, R. Schindler, S. St. Lorant,
K. Thompson, W. Toki, F. Villa, H. Weidner
Stanford Linear Accelerator Center, Stanford, CA 94309

R. Servranckx
TRIUMF, *Vancouver, B.C., Canada*

T. Burnett, V. Cook, R. Mir, P. Mockett
University of Washington, Seattle, WA 98195

Submitted for Publications

* This work was supported in part by the Department of Energy contracts DE-AC03-81ER40050 (CIT), DE-AM03-76SF00010 (UCSC), DE-AC02-76ER01195 (U.Illinois), DE-AC02-76ER03069 (MIT), DE-FG06-85ER40224 (U.of Oregon), DE-AC03-76SF00515 (SLAC), and National Science Foundation grants PHY-8813018 (U.of Cincinnati), and PHY-8822028 (U.of Washington).

TABLE OF CONTENTS

I. INTRODUCTION 3

A. PARTICLE PHYSICS GOALS AND DESIGN PHILOSOPHY 3

B. DESIGN HISTORY 3

C. GENERAL DESCRIPTION 4

II. DESCRIPTION OF THE STORAGE-RINGS 6

A. LATTICE, BEAM SIZES AND LUMINOSITY 6

B. INTERACTION REGION 7

C. MAGNET SYSTEM 8

D. VACUUM SYSTEM 11

E. INSTABILITY CONTROL 13

F. RF SYSTEM 15

G. BEAM MONITORING AT THE COLLISION POINT 16

III. DESCRIPTION OF THE INJECTION SYSTEM 18

A. INTRODUCTION 18

B. SYSTEM 1: 2.5 GEV SLED LINAC 20

C. SYSTEM 2: 2.5 GEV NON-SLED LINAC 20

D. SYSTEM 3: 2.5 GEV LINAC WITH POSITRON & ELECTRON ACCUMULATOR RING 21

E. SYSTEM 4: NON-SLED LINAC WITH POSITRON & ELECTRON ACCUMULATOR FOLLOWED BY BOOSTER SYNCHROTRON 21

F. COMPARISON OF THE FOUR INJECTION SYSTEMS 22

IV. PHYSICAL PLANT 22

A. GENERAL FEATURES AND COLLIDER HOUSING 22

B. COLLIDER HALL 22

C. SHIELDING REQUIREMENTS 23

V. PRELIMINARY COST ESTIMATE 23

VI. SUMMARY 25

ACKNOWLEDGEMENT 25

REFERENCES 25

FIGURE CAPTIONS AND FIGURES 27ff

I. INTRODUCTION

A. *Particle Physics Goals and Design Philosophy*

There is a tremendous need[1-6] for an electron-positron collider which can produce very large numbers of tau leptons and D mesons at energies where the properties of these particles can be studied with high precision and good understanding of experimental errors. This need can be met by the tau-charm factory,[1,2] a two-ring e^+e^- collider with a dedicated injector shown schematically in Fig. 1. The racetrack-shaped storage rings are separated vertically and meet at a single interaction point. The main operating range of the tau-charm factory would be $3.0 \leq E_{cm} \leq 4.4$ GeV covering the physics range shown in Fig. 2.

The design goals are:

(a) maximum peak luminosity of 10^{33} cm^{-2} s^{-1} in the region $1.9 \leq E_{beam} \leq 2.2$ GeV;

(b) rings capable of operating over the range $1.5 \leq E_{beam} \leq 2.5$ GeV;

(c) close to full year use of the collider;

(d) reliable day-to-day operation.

The meeting of these goals requires a dedicated e^+ and e^- injector, conservative solutions to all technical questions, and careful, quality construction. These goals have led us to a design philosophy in which we take the simplest designs that came out of the Tau-Charm Factory Workshop[3] and examine their technical aspects and costs.

Although this document is concerned with the technical characteristics of the tau-charm factory, we note that this 10^{33} cm^{-2} s^{-1} design has an additional conservative aspect in the particle physics reach of the proposed facility. At 2.2 GeV the design luminosity of the BEPC[7] is 1.0×10^{31}, Fig. 3. Hence, even at turn-on the tau-charm factory, with an initial luminosity of 10^{32} to $3{\times}10^{32}$ cm^{-2} s^{-1}, will have 10 to 30 times the luminosity of the BEPC.

B. *Design History*

The design of a circular tau-charm factory began with the seminal work of Jowett.[2] His and other designs were examined at the May, 1989 Workshop.[3] The machine design conclusion of the Workshop was:[8]

> "Overall conclusions from the machine design part of the workshop were that all, or nearly all, of the ingredients for a τ-charm Factory with average

luminosity greater than 10^{33} cm^{-2} s^{-1} exist. The challenge is to assemble them into a working machine. On top of this, several exciting new ideas for even greater luminosities, most notably the 'crab-crossing', moved several steps closer to realization at the workshop."

"If a tau-charm factory project is to succeed then – like any particle 'factory', whose very *raison d'être* is the provision of high luminosity – it must not fall short of its design performance. Such machines cannot redeem themselves simply by virtue of having opened up a new energy region. It follows inexorably that there is no room for compromises or shortcuts: careful and thorough design and engineering will be mandatory throughout the project."

This conclusion and the tremendous particle physics power of a tau-charm factory led to our organizing a collaboration to design the collider and accompanying detector. This document describes the work done as of December, 1989. This work includes: design of a lattice including sextupoles; several preliminary injector designs; preliminary design of housings for the injector, collider, and detectors; radiation safety studies; selection of a preferred RF system for the collider; evaluation of power and other utility needs; and a first cost estimate.

For this design work we set the maximum peak luminosity at $E_{beam} = 2.2$ GeV. Although it may well be set at a lower energy in a final design, this choice puts the most stringent requirements on the RF system and the vacuum chamber.

C. *General Description*

Table 1 gives the general parameters of the collider. It is instructive to compare the parameters of the tau-charm factory with SPEAR, in order to see where the increase in luminosity is being achieved. The luminosity, assuming optimum coupling, is

$$L = \frac{I\gamma\xi_y}{2er_e\beta_y^*}\left(1+\frac{\sigma_y^*}{\sigma_x^*}\right)$$

Since both the tau-charm factory and the SPEAR beams are approximately flat, the luminosity $L \propto (I\xi_y/\beta_y^*)E$. The improvements in luminosity are due to:

(a) *Increased beam current.* With many bunches and an increased emittance, the improvement in I (at 2.2 GeV) is 500 mA: 10 mA, i.e. a factor 50.

(b) *Increased beam-beam tune shift.* The improvement expected in ξ_y is 0.04: 0.025, i.e. a factor 1.6.

(c) *Reduced* β_y^*. The improvement in β_y^* is 1 cm: 10 cm, i.e. a factor 10.

These factors combine to give an overall luminosity increase over SPEAR of about 800.

Table 1. General parameters of the collider at maximum luminosity Energy of 2.2 GeV

Energy	E	2.2 GeV
Circumference	C	329.9 m
Revolution frequency	f_o	0.909 MHz
Bending radius	ρ	12 m
β-function at IP	β_x^*	0.2 m
	β_y^*	0.01 m
Betatron coupling	κ^2	.05
Betatron tunes	Q_x	8.87
	Q_y	7.76
Momentum compaction	α	0.0396
Natural emittance	ϵ_x	424 nm
Fractional energy spread	σ_ϵ	5.44×10^{-4}
Energy loss per turn	U_0	0.173 MeV
Damping times	τ_x	28 msec
	τ_y	28 msec
	τ_ϵ	14 msec
RF frequency	f_{RF}	500 MHz
RF voltage	V_{RF}	24 MV
Radiated power per beam	P_{rad}	86 kW
Number of bunches	k_b	21
Bunch separation	S_b	15.71 m
Bunch spacing	τ_b	52.4 ns
Bunch crossing frequency	f_b	19.1 MHz
Total beam current	I	498 mA
Particles per bunch	N_b	1.63×10^{11}
r.m.s. bunch length	σ_z	6 mm
Beam sizes at IP	σ_x^*	284 μm
	σ_y^*	14 μm
Beam-beam parameter	ξ_y	0.04
Luminosity	L	1.0×10^{33} cm^{-2}s^{-1}

II. DESCRIPTION OF THE STORAGE-RINGS

A. *Lattice, Beam Sizes, and Luminosity*

The collider consists of two rings, one above the other, with one interaction point (IP). Each ring is 48 m wide and 139 m long with a circumference of 330 m. For the design luminosity of 1.0×10^{33} cm^{-2} s^{-1} at 2.2 GeV beam energy: there are 21 bunches with about 1.6×10^{11} particles per bunch, the total current per beam is 500 mA and the interbunch spacing is 15.7 m.

Figure 4 shows the lattice of half of one ring. One long straight section (utility straight) contains the wigglers and one half of the RF cavities (76 m total). The opposite straight section (insertion straight) contains the interaction point, $\mu\beta$ insertion and electrostatic vertical separators (15 m total); the vertical separation section ($2 \times$ 21 m total); and the straight sections (2×9.5 m total) containing the remaining half of the RF cavities. Each arc contains 3 cells, each giving a 10° bend, followed by 6 cells, each giving a 20° bend, and then 3 cells, each giving a 10° bend. The dipoles have a 12 m bending radius. Figure 5 gives the β functions and other lattice parameters calculated using DIMAD, and Fig. 6 gives the beam envelopes in units of 10σ.

The lattice is designed for stability under the following conditions:

transverse errors ≤ 300 μm
longitudinal errors ≤ 3 mm
field setting errors $\leq 10^{-3}$

The stable region covers 20σ in each transverse dimension and 10σ in momentum. This is achieved with a simple orbit correction scheme. The residual rms orbit distortions are less than 400 μm in each transverse plane. The maximum orbit displacement is less than 1 mm. These results are achieved using 70 orbit correctors and 35 position monitors.

The horizontal and vertical tunes are 8.873 and 7.762, respectively. Half quadrupoles are used at present to terminate the cells in the design procedure; in the final design the halves will be refitted to make a single magnet. In the present design, one family of sextupoles per plane is used. This corrects the chromaticity but not the momentum dependence of the beam size at the IP. The final design can use up to three sextupole families, providing 60° per cell is maintained.

Figure 7 shows the design luminosity as a function of E. Using the wigglers, an E^2 dependence is obtained below 2.2 GeV. Above 2.2 GeV, the luminosity is limited by a maximum current of 500 mA per beam. The average luminosity will be maintained at 75 to 80% of the peak luminosity. The lifetime due to interactions of the beam with residual gas in the ring is 8 hrs. The lifetime due to $e^+e^- \rightarrow e^+e^-\gamma$ is shortest at the maximum beam current; it is 3.4 hrs. at 500 mA beam. Hence, the shortest combined lifetime is 2.4 hrs. The ratio of average to peak luminosity of 75% is obtained by topping off the beams every 65 min. allowing 4 min. for all injection. Injection every 30 min. would increase the ratio to 80%.

B. Interaction Region

The interaction region in the tau-charm factory is conventional, with a large diameter (12 cm ID) vacuum chamber. Physics in the tau-charm threshold region does not require a small beam pipe; indeed, the physics performance improves with a large pipe. The 12 cm beam pipe matches the aperture requirements of the $\mu\beta$ quadrupoles, simplifies the masking of synchrotron radiation and minimizes the impedance. At the IP, $\sigma_x = 284$ μm, $\sigma_y = 14$ μm, and $\sigma_E/E = 5.4 \times 10^{-4}$. These small values are very useful in the particle physics research at the tau-charm factory.

The beams are brought together and separated using electrostatic fields. As shown schematically in Fig. 8, on each side of the IP is a superconducting $\mu\beta$ quadrupole triplet beginning 80 cm from the IP. The outer radius of the $\mu\beta$ quadrupole triplet is 20 cm. The quadrupole parameters are given in Table 2. The maximum quadrupole strength is $|K| = 2.87$ m^{-2}. At 2.5 GeV this corresponds to a field gradient $dB/dx =$ 24 T m^{-1}. With a half-aperture of 70 mm, the pole-tip field is 1.7 T.

Table 2. Properties of insertion quadrupoles

Name	Q1	Q2	Q3	Q4
Type	super-conducting	super-conducting	super-conducting	room temperature
Bore Diameter (mm)	140	140	140	140
Length (m)	0.6	0.6	0.6	0.6
K(m^{-2})	–2.87	+2.66	–1.05	+0.79

Electrostatic separator designs have been discussed by Jowett[2] and by Donald and Garren.[9] The space provided for each separator is 4 m, extending from 3.5 m to 7.5 m from the IP. This 7.5 m defines half the bunch spacing; it is the location of closest approach between the bunch that has just left the IP and the bunch that is about to enter the IP. The quadrupole triplet design gives a small bunch height at this point, $\sigma_y \approx 0.5$ mm.

The plate separation and voltage are determined as follows. We require a bunch vertical separation of 40 σ_y (20 mm) at the outer edge of the separators, which implies an electric field of 2.8 MV m^{-1}. Between each bunch and the nearer plate, we require an additional space of 10 σ_y (5 mm) + 5 mm (orbit excursions) + 20% = 12 mm. Finally, a further 13 mm is added for each bunch, to allow operation with well-separated beam orbits (26 mm). The half-separation of the electrostatic plates is therefore 10 + 12 + 13 = 35 mm, i.e. a total plate separation of 70 mm. The required plate voltage is therefore $\pm 0.5(2800 \times .07) = \pm 100$ kV. Figure 9 shows schematically how the final vertical distance between the beams, 1.2 m, is obtained beyond the electrostatic separators.

C. *Magnet System*

1. General Description

The tau-charm storage rings are separated function rings. Magnetically, each ring contains 24 bend cells divided between 12–10° cells and 12–20° cells, and 18 standard straight cells. The 10° bend cell contains two 5° bend magnets, two halves of a focusing quadrupole, a defocusing quadrupole, a pair of sextupoles and a vertical steering corrector. The 20° bend cell is different only in that it contains two 10° bend magnets instead of the 5° magnets. Typical bend cell configurations are shown in Fig. 10. The standard straight cell consists of two halves of a focusing quadrupole, a defocusing quadrupole, and horizontal and vertical steering correctors. The total magnet complement for each ring consists of 24-5° and 24-10° bend magnets, 45 focusing and 45 defocusing quadrupoles, 48 sextupoles, and 70 steering correctors.

The bend magnets in each ring are connected in series to a common power supply. In the arcs, all the focusing quadrupoles are connected in series to one power supply, as are the defocusing quadrupoles. Other magnets will be individually powered. A brief description of each magnet follows: All water cooled coils in the main rings are made of hollow aluminum conductor. Use of one material in contact with cooling water in each cooling system will minimize corrosion problems. The coils will be fully vacuum

potted using a traditional epoxy-glass insulation system for reliability.

2. Dipoles

The dipoles will be solid core "H" magnets. "C" magnets are not necessary because synchrotron radiation levels are sufficiently low to allow traditional means of cooling the vacuum chamber wall. The "H" configuration has several inherent advantages over "C" magnets: it provides greater rigidity, allows for a smaller cross section, and is generally less costly.

Two lengths of main ring horizontal bend magnets are used. The 2 meter long magnets bend the beam through 10 degrees while the 1 meter long magnets bend the beam through 5 degrees. In all other respects these magnets are the same. The magnets have a 10 cm high gap. The required field strength is low, 6.9kG. Poles are flat and have a pole width of approximately 32 cm. The wide pole is needed to provide a good field region to cover the 11.4 mm sagitta of the 10 degree magnet. Forty-eight of each of these magnets are needed for the two rings. Coils are wound of 1 inch square hollow aluminum conductor. Coils are wound flat and then the ends are "humped" to clear the beam pipe. All the bend magnets for both rings are connected in series and are powered by a single power supply. All magnets have individually powered trim coils which can add or subtract up to 3% of the field strength.

3. Quadrupoles

Two quadrupole designs will be used in the ring; one for the quadrupoles in the arcs and straight sections and a larger bore design for the insertion quadrupoles. The main ring quadrupoles have a 10 cm diameter bore. Cores are machined from solid 1008 or 1010 steel slabs and bars. Coils are "race track" type using .42 inch square aluminum conductor with a .187 inch diameter cooling hole. 180 quadrupoles are required. They are all connected in series to a common power supply. Each quadrupole has individually powered trim coils which can add or subtract 3% to the quadrupole strength.

Three of the four insertion quadrupoles will be superconducting, and one will be warm. These will have a bore diameter of 140 mm, Table 2.

4. Sextupoles and Steering Correctors

Sextupoles also have a 10 cm diameter bore. Cores are laminated. Coils are 3 dimensional, wound of #10 (.108 inch) square copper conductor. Coils are air cooled. All 180 sextupoles are connected in series to a common power supply. It is possible

that sextupoles are needed only in the arcs. In that case only 96 sextupoles are needed. The cost estimate is based on 180 magnets.

Steering correctors have a 10 cm high gap. Their poles are 15 cm wide. Cores are solid. Coils are flat and are made from #10 square copper conductor. Their strength is equal to that of the 10 degree bend magnet trim. Ninety-six correctors are required in the arcs for vertical steering. The remaining 44 are distributed in the straight sections and are used for both horizontal and vertical steering. Correctors are individually powered.

5. Insertion Magnets for Interaction Region

An elevation view of the insertion area is shown in Fig. 9. Six vertical bend magnets on each side are "C" magnets so that they can be placed close together. Each magnet is capable of bending the beam by 5.7 degrees. The two magnets closest to the IP must bend both beams and require a special design. Required field strength is 5.5 kG. Cores are machined from 1010 steel slabs. Magnet gap is 10 cm. Pole width is 30 cm. Coils are wound of 1 inch square hollow aluminum conductor having a .375 inch diameter cooling hole. All insertion bends are connected in series and are powered by a single power supply. Each bend magnet has a 3% trim coil which is individually powered.

6. Support System for Ring Magnets

All arc beam line components will be supported from girders. There will be two girders per bend cell. Arc quadrupoles, sextupoles, steering correctors and any beam diagnostic instrumentation will be mounted on girders and aligned in the shop. Complete girder assemblies will then be transported to and installed in the tunnel. Preassembly will save installation and alignment time in the tunnel. Horizontal bend magnets are supported from the ends of adjacent girders. Girders for both rings are supported near their ends by stanchions. In this way, the weight of the heavy bend magnets is transmitted directly to the stanchions and does not contribute to deflecting the girders. Stanchions will be bolted and grouted to the floor and bolted to the wall for earthquake stability. Arc component positions on girders are shown in the arc bend cell elevation view, Fig. 11.

Components in the straight sections, including the insertion regions, can be mounted on girders and stanchions in the same way as the arc components.

7. Transport Line from Injector to Main Ring

A brief study of the transport line requirements shows that we can copy the design of the Linac-to-PEP transport system at SLAC. Each transport line consists of 8 bend magnets and 16 quadrupoles. The first bend magnet after the linac is common to both the e^- and e^+ transport lines.

Each bend magnet bends the beam through 11.25 degrees. The gap full height is 5 cm. The pole width is 15 cm. Coils are wound of 1" square aluminum conductor having a .375 inch cooling water hole. All transport bend magnets are powered in series from a single power supply. Transport line quadrupoles have a 5 cm diameter bore. Coils are wound of .187 inch square hollow conductor. The quadrupoles have individual power supplies.

D. Vacuum System

1. Dimensions

The vacuum chamber dimensions have been determined according to the following criteria:

a. A minimum inner half-aperture (radial dimension) equal to 10 $\sigma_{x,y}$ + 5 mm (orbit excursions) + 10–20% (safety factor).

b. An outer radial dimension equal to the inner dimension+ 5 mm (Al wall) + 5 mm (insulation). For example, a cylindrical chamber of 80 mm ID requires a magnet bore of 100 mm.

c. As few variations in size as possible, in order to result in the minimum impedance.

The vacuum chamber will be made from both straight and curved extruded aluminum sections with the following inner dimensions:

Interaction region and $\mu\beta$ quads:	120 mm diameter, circular
Arcs, utility straight sections and vertical separation sections:	80 mm diameter, circular

A 5 mm radial clearance has been allowed between the outside of the vacuum chambers and the magnet apertures. This space can be used for insulation in the event that the vacuum system needs to be baked in place. The vacuum chamber would be heated through its water cooling passage.

2. Vacuum Quality

A vacuum pressure, with beam, of 5 nTorr is sufficient to provide a long lifetime ($\sim$ 8 hours) for coasting beams. This is the operational value at PEP and is straightforward to achieve. The actual luminosity lifetime will be 2.4 hours, dominated by beam-beam bremsstrahlung losses.

The synchrotron power load is 86 kW per ring, or, equivalently, 11.4 W per cm of arc. It is straightforward to handle such loads with water-cooled vacuum chambers in the arcs; the PEP vacuum chamber, for example, is designed for 46 W cm^{-1}. Therefore, existing technology, which was used to design and construct the SPEAR and PEP vacuum systems, can be used. A cooling water passage is located on the outside of the vacuum chamber to remove synchrotron radiation heat.

The critical energies of the synchrotron photons are very low: 2.0 keV from the main bends and a maximum of 4.0 keV from the $\mu\beta$ quads. Such photons can be efficiently masked in the interaction region to prevent their reaching the detector.

Transport line vacuum requirements are modest. Therefore, only limited pumping capacity will be provided. The transport line vacuum will be separated from the ring vacuum by a short air gap with thin beam windows on either side.

3. Ring Impedance

The most critical aspect of the vacuum chamber design is to minimize the longitudinal impedance $|Z/n|$ so that short bunch lengths are maintained. The tau-charm factory is designed to have a bunch length $\sigma_z = 6$ mm in order to match the strong vertical focusing ($B_y^* = 1$ cm) at the interaction point. The Keil-Schnell-Boussard criterion for the absence of turbulent bunch-lengthening indicates that the longitudinal impedance at the peak energy of 2.2 GeV must be,

$$|Z/n| \leq 0.3\ \Omega \quad .$$

To achieve this value will require careful design of a smooth vacuum chamber and the use of RF cavities with a smoothed shape. A large circular vacuum chamber with an 8 cm inside diameter is used throughout the arcs and straight sections. The transition to the 12 cm inside diameter vacuum chamber through the insertion quads will have to be very smooth and gradual. Use of a round vacuum chamber makes the magnet gaps larger than would be dictated by beam-stay-clear considerations alone. The larger

gaps, of course, make the magnets larger, more expensive, and more costly to operate. We will follow the LEP solution for bellows shields with sliding contacts. Pump-out ports need to be shielded and the beam position monitors must have small impedance. In summary, the low impedance of 0.3 Ω can be achieved, as demonstrated, for example, by the preliminary measurement of 0.1 Ω at LEP.

Finally, we comment that a system is required for clearing the positive ions trapped in the e^- ring. Possible cures involve electric clearing fields (of a few hundred V cm^{-1}) or an uneven bunch spacing, which generates a periodic kick that displaces the ions from their potential well.

E. Instability Control

1. Multibunch instabilities

The tau-charm factory design has a total current of about 0.5 A, distributed into 21 bunches spaced by 15.7 m. Thus, coupled-bunch instabilities are a potentially serious problem and are an important consideration in the design of the ring; in particular, it is essential to minimize the impedance of the RF system.

An RF system utilizing an example of a superconducting cavity shape was assumed in the present calculations. Such a cavity has a large aperture, which reduces the number of parasitic modes trapped within it. In addition to the fundamental accelerating mode, there are two parasitic longitudinal modes and two parasitic transverse modes in this cavity.

An RF system at high frequency (1500 MHz, the frequency used in the initial Jowett design) and low frequency (350 MHz) was studied. The motivation for considering a lower frequency is to reduce the impedance and thus the beam instabilities. The RF system was assumed to consist of 24 cells, which is what is required to obtain sufficient voltage to maintain the short bunch length, assuming an accelerating field gradient of 4 MeV/m. This is true for either the higher or lower RF frequency.

The Q's of the parasitic modes may be much reduced by using HOM couplers; the reduction can be about a factor of 100 below the Q's calculated (using the program URMEL) for copper walls alone. Thus the instabilities were calculated for Q's ranging between these two extremes.

An additional factor that should be taken into consideration in calculating the instability is the possibility of a cavity-to-cavity spread in the frequencies of corresponding

higher-order modes. Such a spread reduces the largest instability growth rates if it is sufficient to keep the resonance lines in different cavities from overlapping. The instabilities were calculated for a total spread of up to 1% in the frequencies of the parasitic modes.

A "normal-modes" approach[10-11] was used to calculate the coherent frequencies Ω of the 21 modes of coupled-bunch oscillation, in both the longitudinal and transverse directions. The imaginary part of each coherent frequency gives the growth or damping rate of the corresponding oscillation mode. The maximum growth rates give an indication of the requirements on the feedback systems to control the instabilities. At the tau-charm factory energy, it is reasonable to expect that instabilities with characteristic growth times $1/Im\Omega$ of about a millisecond or more can be controlled via feedback.

Results for the maximum instability growth rates $Im\Omega$ are shown in Figures 12a through 12d. The horizontal axis in each of these plots is the factor by which the Q's of the parasitic cavity modes are reduced from the Q's for copper alone. The maximum growth rate of all the 21 coherent modes of coupled-bunch oscillation is plotted vertically. In calculating the longitudinal growth rates, we have assumed that the frequency of the fundamental longitudinal mode is slightly less than the harmonic number times the revolution frequency, as would be the case in normal ring operation.

Figures 12a, b and c show the longitudinal growth rates, assuming frequency spreads of the parasitic cavity modes of 0%, 0.1% and 1.0%, respectively. Points are plotted for high (1500 MHz) and low (350 MHz) frequency. At the higher frequency, the growth rates are faster than the value 10^3 sec^{-1} deemed reasonable for the feedback system, Even the maximum assumed Q reduction and frequency spread are not quite sufficient to bring the growth time down to a millisecond. A combination of moderate Q reduction and/or frequency spread is seen to bring the growth rates comfortably below 10^3 sec^{-1}, in the low frequency case. This is the main motivation for going to a lower RF frequency.

In Figure 12d, the transverse growth rates are plotted, assuming a 1.0% spread in frequencies of the parasitic cavity modes. Here a Q reduction of about 10 for the low frequency case and somewhat more for the high frequency case is needed.

2. Other instabilities

As noted earlier, the requirement for avoiding the turbulent bunch-lengthening instability is $|Z/n| \leq 0.3\Omega$. This is obtainable with careful design of the vacuum

chamber and RF system, to minimize the impedance.

Assuming that this low value of Z/n is achieved, one will also be well below the threshold $Z_\perp \sim 1.4\text{M}\Omega/\text{m}$ for the transverse mode-coupling instability, even for vacuum chamber radius b as small as 1.0 cm. Thus, the mode-coupling instability will not be a problem.

F. *RF System*

1. Selection Criteria

We considered three options for the RF system:

a. 1200–1500 MHz superconducting cavities.

b. 350–500 MHz warm cavities.

c. 350–500 MHz superconducting cavities.

In the original Jowett machine design, an RF frequency of 1500 MHz was chosen as an initial approach to achieving the desired short bunch length. However, this choice was made before studying single- and multi-bunch effects, which are strongly reduced at lower RF frequencies. Our approach to these instabilities – which will limit the ultimate performance of the tau-charm factory – is first to minimize their inherent contributions by optimized machine design and *then* to apply active feedback systems for their control. In the light of a study of beam instabilities, we therefore selected a reduction of the RF frequency to 500 MHz, along with a corresponding increase in the total voltage per ring to 24 MV in order to achieve a bunch length of 6 mm.

Having selected 500 MHz we then decided on superconducting as opposed to warm cavities. The use of *warm* low-frequency cavities results in considerable power requirements (16 MW total) despite the modest accelerating voltage (173 keV) and modest power (172 kW total) required by the beams. The large RF voltage (28 MV) is only needed to provide sufficient slope of the RF wave to maintain a short bunch length $\sigma_z =$ 6.0 mm. These conditions are ideally suited to the use of superconducting RF cavities. In addition to the sharply-reduced power requirements, there are several further advantages in using superconducting RF cavities. They provide a larger accelerating voltage gradient, which leads to fewer cavities for a given total voltage, and therefore results in a lower machine impedance. Furthermore, their large Q allows the use of a very smooth cavity form with a large beam port, thereby reducing the parasitic impedance due to higher order modes and improving the stability of high intensity bunches. Couplers

are required to attenuate higher order modes and thereby reduce the beam instabilities and decrease parasitic power dissipation at liquid He temperatures. Couplers have been designed and built for both the LEP and HERA cavities, but they have so far only been tested at low beam currents.

2. Parameters of RF System

A separate report is being written on the RF system.

3. Refrigeration

The tau-charm cryogenic system would consist of a helium refrigerator plant at the site with a capacity of 200W at 4.2K. Following industrial practice, the local plant will be configured as two systems: an atmospheric (4.2K) refrigerator/liquifier module and a sub-atmospheric module with cold compressors and associated equipment for 2K operation, if required. Both modules are available as "off-the-shelf" refrigerators, complete with controls. The cryogen distribution system will consist of rigid and flexible shielded transfer lines of the type currently in use at SLAC, and a number of liquid nitrogen and helium storage tanks and dewars.

G. *Beam Monitoring at the Collision Point*

Initially the e^+ and e^- beams must be brought into collision and then their alignment must be maintained with a transverse precision better than $0.1\sigma_{x,y}$, where σ_x (284 μm) and σ_y (14 μm) are the transverse beam sizes at the interaction point. Special attention is required to achieve this stability – especially in the vertical plane where the beams must be maintained to a relative accuracy of 1 μm – due to the presence of two independent rings. In a single-ring collider, drifts in the lattice components tend to affect both beams equally and therefore largely cancel. In order to simulate single-ring conditions as closely as possible, the τcF storage rings should be mounted on rigid supports in a stable tunnel, and corresponding magnets in each ring should be powered from the same supply.

The proposed scheme for beam alignment at the interaction point is as follows: The e^+ and e^- bunches are initially brought into collision by measuring the beam-beam deflection with beam position monitors (BPM's) near the interaction point. Bhabha scattering ($e^+e^- \rightarrow e^+e^-$), which is measured in the small-angle monitors of the τcF detector, subsequently provides active feedback for automatic fine transverse adjustments of the beam during data taking. During the initial tuning, the beam-beam deflection

is also used to adjust the horizontal and vertical focal points of the $\mu\beta$ quadrupole triplets (the beam 'waist') precisely to the crossing-point. Longitudinal stability is subsequently provided by phase-locking of the RF systems of the two storage rings. We discuss this scheme in more detail below.

Measurements of beam-beam deflections at the SLC[12,13] have proved an excellent technique for tuning and monitoring the beams at the interaction point ($\sigma_{x,y} \simeq 2\mu$m). For large impact parameters, the average vertical deflection angle of one bunch by an oppositely-charged bunch moving in the opposite direction is[12,13],

$$\langle\theta_y\rangle \simeq -\frac{2r_e N_b}{\gamma\Delta_y} \tag{1}$$

where r_e is the classical electron radius, N_b is the number of particles per bunch, γ is the Lorentz factor and Δ_y is the vertical separation between the centres of the two bunches. This expression assumes that the bunches are aligned horizontally and that the vertical separation is large compared with the transverse dimensions of each bunch, i.e. $\Delta_y \gtrsim 3\sigma_x$. As the separation decreases, there is an increase in the deflection angle until it reaches a maximum value which, in the case of round beams ($\sigma_x = \sigma_y$), occurs when the bunches partially overlap, $\Delta_y = 2.3\sigma_y$.[12] As the separation is reduced still further, $\langle\theta_y\rangle$ decreases linearly with Δ_y until it is zero when the beams are perfectly aligned, $\Delta_y = 0$. The slope of this linear region can be used to measure the transverse dimensions of the bunches at the crossing point. Numerically, expression (1) indicates $\langle\theta_y\rangle$ [mrad] $= -0.21/\Delta_y$ [mm] for the τ-charm Factory at $E_b = 2.2$ GeV. For large impact parameters, this is much larger (a factor $\simeq 300$) than at the SLC, due to the smaller energy (factor 20) and larger number of particles per bunch (factor 15).

The beam position is measured near the SLC interaction point with a relative accuracy $\sigma_{x,y} = 10$ μm for *each bunch* of 5×10^9 particles. These measurements are made with sets of x- and y-measuring BPM's[14] located inside the final-focus $\mu\beta$ triplets, at 2.8 m and 4.0 m on each side of the interaction point – four sets in total. At the τ-charm Factory, although the BPM's would be closer to the interaction point (less than 3.2 m), we anticipate similar accuracy could be achieved due to the larger bunch charge. By averaging up to 100 bunches, a precision of 5 μrad can be achieved on the relative deflection angle. Using equation (1), this indicates that the beam-beam deflection is measurable for large impact parameters $\simeq 1$ cm and will therefore be useful for initial adjustments as well as precise final alignment.

The procedure is first to centre, say, the e^- beam without any e^+ beam. In fact, with carefully designed and calibrated BPM's[14] this can probably be done with an absolute accuracy $\sigma_{x,y} = 100$ μm. The e^+ beam is then centered in the absence of an e^- beam, without disturbing the common optics of the $\mu\beta$ insertion. Finally the two beams are measured together, and the changes in the BPM values measures their deflections. The SLC experience with this technique indicates that the beams can be transversely aligned with a precision of better than 10% of their widths. Furthermore, by scanning the beam-beam deflections at several different focal strengths of the final-focus quadrupoles, the beam waists in the vertical and horizontal planes can be adjusted to coincide within 1 mm of the interaction point.[13] This precision is perfectly adequate for the τ-charm Factory, where the bunch length is $\sigma_z = 6$ mm.

After initially setting up the beams in this way, the collision point is monitored by means of the Bhabha scattering signal measured in the small angle monitors of the τcF detector. The large Bhabha rate, 4 kHz, implies that the luminosity can be measured with 1% accuracy in each 3 second interval. Consequently, drifts in the luminosity at a rate $\lesssim 1$ Hz can be kept below 1% by suitable active feedback systems. The azimuthal distribution of events in the luminosity monitors will also provide useful information to confirm that the interaction point remains transversely centered. Finally, once the beams are transversely aligned, measurement of the luminosity provides a second technique to tune the beam waists at the interaction point.

III. DESCRIPTION OF THE INJECTION SYSTEM

A. *Introduction*

In this section we describe four different injection systems. When this design work was carried out, SLAC was a possible site for a tau-charm factory and there was an emphasis on systems using only linear accelerators and accumulator rings. It may be that the fourth system discussed here, which uses a booster synchrotron, is most suitable for other sites.

Four alternative injection systems for the tau-charm factory have been studied. Their configurations and main characteristics are summarized in Fig. 13. The first two systems use pure linacs, the third one uses linacs combined with an accumulator ring, and the fourth one uses linacs followed by an accumulator ring and a booster synchrotron. The four injectors are presented in order of increasing cost, ranging between

$20 and $30 million. The times required to fill the tau-charm factory with electrons and positrons from zero to full current ("full-fill" mode) range from 3.5 minutes for System 1 (probably not acceptable) to 33–77 seconds for System 2, 3 and 4. These filling times do not include transitions to switch from one particle to another, "off" times for drift chambers and background decays, etc. On the other hand, these times are shorter in the "top-off" mode rather than in the "full-fill" mode. The two-ring tau-charm factory has the advantage that the two beams do not "see" each other, except near the IR. Consequently, neither the order in which particles are filled nor the exact bucket filling procedure is too critical, and some flexibility in operation can be preserved until after the machine is constructed and tested.

The common assumptions underlying the filling times shown in Fig. 13 are:

1. The charge per ring at 2.2 GeV is 3.4 $\times 10^{12} e^{\pm}$ (544 nC). This corresponds to $\sim$0.5A of circulating current per beam and 25.9 nC per bunch, given 21 bunches.
2. The pulse repetition rate of the injection systems is limited by the τ_x or τ_ϵ damping times of the tau-charm factory. The following damping times are assumed:

	2.2 GeV	1.6 GeV
τ_x	28 msec	73 msec
τ_y	28 msec	73 msec
τ_ϵ	14 msec	36 msec

Because the stored charges at different energies scale inversely with the damping times, the calculated filling times are roughly independent of energy for systems 1 and 2 where the e^+ source repetition is limited by the damping time of the main ring.

3. The positron yield of the positron source is 2% per incident electron per GeV. Thus, for 0.5 GeV incident electrons, the yield is 1%. The normalized emittance of the positron beam from the linac is $\epsilon_n(e^+) = 5 \times 10^{-3}\pi$ rad - m.
4. The filling efficiency for the tau-charm factory is assumed to be 20% of incident charge from the injection system.
5. Electron injection is accomplished from the front-end gun and a bypass around the positron source, or perhaps from a second off-axis gun installed immediately downstream of the positron source.

   The electron injection filling times are assumed to be 10% of the positron filling times for Systems 1 and 2, and roughly 50% for Systems 3 and 4.

B. System 1: 2.5 GeV SLED Linac

Referring to Fig. 13, this system consists of two linacs, the first with two 64 MW klystrons, the second with ten 64 MW klystrons. Each klystron (with a 3.5 μsec RF pulse) is equipped with two SLED cavities and four accelerator sections yielding approximately 250 MeV of energy. Because of the non-flatness of the SLED pulse, it is assumed that only three bunches spaced 52.4 nsec apart can be accelerated on one pulse. Assuming bunches of 5×10^{10} electrons and the above positron yield, it is easy to calculate that at 60 pps, the "full-fill" time for both rings will take 3.5 minutes. This time is probably unacceptable unless other dead-times are comparable. The system has the advantage of being the simplest and the least expensive because it requires the least number of klystrons and modulators (which dominate the cost). Since only three bunches are accelerated per pulse, filling the rings requires triggering the linac pulses at successive times with respect to the rings.

C. System 2: 2.5 GeV Non-SLED Linac

This system is similar to System 1 except that it does not use SLED cavities. The advantage is that the RF pulses can be flat and a full train of 21 bunches can be accelerated on each pulse. The price one has to pay for this advantage is that the number of klystrons and modulators is doubled even though the number of accelerator sections (and therefore the approximate length) is the same. To achieve the same energy, the klystrons would have to run at 80 MW peak, 2 μsec pulse and 60 pps. This peak power should be achievable because the klystrons have already been tested successfully at 100 MW and a 1 μsec pulse. By producing trains of 21 bunches, each again with 5×10^{10} electrons incident on the e^+ source and a 1% positron yield at 500 MeV, it should be possible to fill the rings in one-seventh of the time given for System 1, or ~ 33 sec. This rate is entirely satisfactory. In order to inject into the rings at 60 pps, it may be advantageous to inject into synchrotron phase space, i.e. on the closed orbit for an off-momentum particle, since the synchrotron damping time is half the betatron damping time.

For single-turn injection, the kickers must have a 1 μsec flat top and rise and fall times shorter than 52 nsec so as not to disturb adjacent bunches. This has almost been achieved in the SLC damping rings. In order to equalize the charges in all bunches in the rings even though the bunches from the linac might not have identical populations, successive linac triggering times can be delayed so as to "walk" the linac bunch trains

around each ring. After the rings are filled, it would also be possible to trim individual bunches by generating single bunches from the gun.

D. System 3: 2.5 GeV Linac with Positron & Electron Accumulator Ring

This system uses a non-SLED linac (500 MeV up to the positron source, and 500 MeV beyond) to produce 300 nsec e^+ or e^- bunch trains which can be injected and accumulated in a 500 MeV accumulator ring. Injection into the accumulator is done at a 60 pps rate. The accumulator collects the particles from 9 consecutive pulses (133 msec), compresses them into one single bunch by means of RF systems (66 msec), and re-ejects them at a 5 pps rate into a 5 pps, 2 GeV SLED linac. With an initial 0.5A peak, 300 nsec electron pulse, again a positron source with a 1% yield at 500 MeV and an average repetition rate of 45 pps and the proper derating factors, the positron "full-fill" time would be 50 seconds. The electron "full-fill" time determined by a stochastic bunch lengthening limit in the accumulator ring of about 5×10^{10} e^-/bunch would be 27 seconds. Thus the total is 77 seconds.

Although the design details of the accumulator have not been worked out, a similar ring (PIA) has been used routinely with great success at DESY for the same purpose. With a circulating time of about 105 nsec ($\sim$ 37 m circumference), a three-turn injection into betatron phase space could be used. The ring would probably have three RF systems, a fundamental at 9.52 MHz, a tenth-harmonic at 95.2 MHz and a third system at 714 MHz. The latter two systems would have to be turned on sequentially to perform the bunch compression adiabatically in the time available ($\sim$ 4/60th of a second). The single bunch would then be ejected from the ring, compressed further by a 2856 MHz linac section (like in the SLC ring-to-linac lines) and injected into the SLED linac. Injection into the tau-charm rings would be done in betatron phase space, one bunch at a time, at 5 pps. Although this is not shown in the figures, for filling with electrons the gun would be turned down by more than an order of magnitude. The beam would bypass the e^+ source and be injected at the proper energy (500 MeV) into the accumulator ring, in the opposite direction.

E. System 4: Non-SLED Linac with Positron & Electron Accumulator Followed by Booster Synchrotron

This system is identical to System 3 from the gun to the output of the accumulator ring. However, after leaving the accumulator, the beams are injected into a 2.5 GeV booster synchrotron. No S-band bunch compressor is therefore required at the output

of the accumulator. The filling times are estimated to be the same as for System 3, i.e. $\sim$ 77 seconds. Although the booster synchrotron has not yet been designed, it should be quite conventional.

F. *Comparison of the Four Injection Systems*

Of the four systems described here, System 1 is clearly the simplest and least costly. Systems 2 and 3 are roughly equivalent in cost, and System 4 is probably the most expensive. Because System 1 gives too long a filling time, the optimum choice seemed to be between Systems 2 and 3. We selected System 3 for the cost estimate (see Section V below) because System 2 is based on using a train of bunches, which may not be as convenient and flexible as filling with one bunch at a time.

IV. PHYSICAL PLANT

A. *General Features and Collider Housing*

In our design we proposed that the collider and injector be built underground for radiation shielding and ease of construction. This also gives a flat site above the ring for utility and other auxiliary buildings.

A sketch of the collider housing is shown in Fig. 14. The positron and electron storage rings for the collider will be installed in a common concrete housing constructed in a trench and covered with 1.8 m of earth. The housing is oval with semicircular ends of 24.2 m radius; the long axis of the oval is 139.4 m. It is 3.8 m high and 4 m wide. The housing is in a horizontal plane. On one side the housing opens into the interaction region pit.

For our injector housing design, Fig. 15, we used System 3, Sec. III.D, as an example. The three sections of the linear accelerator, the accumulator ring and the beam transport lines to the collider are installed in concrete housings constructed in excavations and covered with 2.1 m of earth. The total length of the linear accelerator sections is about 150 meters. The accelerator housing is 2.7 m high and 3.0 m wide. The housing for the accumulator is a rectangular vault 3 m high, 11 m wide, and 18 m long. All the underground housings are at approximately the same elevation.

B. *Collider Hall*

Our design envisioned a collider hall which could house two detectors, one on-line and one off-line. Figures 16 and 17 show the proposed hall. The detector pit is

7.8 m deep, 14 m wide and 48.5 m long. The pit has three sections: one on-line detector position and two off-line spaces, at each side. The collider hall building is 60.5 m long, 20 m wide and 14 m high. Two 50 ton overhead bridge cranes provide coverage of the entire pit and of a loading apron at ground level. One wing of the hall has space for control rooms, shops, and offices.

C. *Shielding Requirements*

Shielding of the injector and collider will be determined primarily by beam current and running times. It is assumed that the injector will run for greater periods than simply required to fill the collider ring, and thus should be shielded accordingly. The criteria to be satisfied will be to limit dose rates and annual doses to regions just outside the shield (i.e. the shield surface, or the office spaces adjacent to the collider hall) to less than 3 rem per 6000 hour operating year (0.5 mrem/h). For the collider, where the number of electrons/yr is fairly well known, the shield thickness would be about 1.75 m concrete equivalent. The shield thickness of the injector would probably be less than 2 m concrete equivalent with additional local shielding provided around the positron source. In the interaction region the detector would be self-shielding with additional shields to be added to the beam pipe between the collider tunnel and the detector.

V. PRELIMINARY COST ESTIMATE

When a new accelerator or collider is proposed, one of the first questions is, "What will it cost?" On the basis of the design in this paper we have made a first, crude estimate of the construction cost. We warn the reader that this cost is indeed crude and preliminary. We did not have time to do engineering in detail, nor was there time to have the cost estimates reviewed by others. Furthermore, costs vary with the site and with the countries where the parts of the collider are built. Finally, different countries use different cost accounting systems; we used the system required by the United States government which includes all labor costs.

We find a total cost of 107 million U.S. dollars in 1989 prices. Table 3 gives the individual items. The costs include engineering, design, and inspection (ED&I) as well as construction, but not contingency or inflation. The conventional facilities cost is most site-dependent. For example, the 21 M$ for utilities depends on the proximity and type of the primary electric power supply. This cost was for a site we studied at SLAC.

Table 3. Preliminary, approximate cost estimate for the tau-charm factory. The costs are given in millions of 1989 U.S. dollars. Neither contingency nor inflation corrections are included.

1.	Room Temperature Magnets		
	main ring magnets fabrication	3.67	
	ED&I at 15%	.55	
	Subtotal		4.2
2.	Mechanical Assembly and Installation	1.20	
	ED&I at 15%	.18	
	Subtotal		1.4
3.	Superconducting Quadrupoles and Separators		
	fabrication, assembly, supports, sensors, and installation	1.25	
	ED&I at 30%	.38	
	Subtotal		1.6
4.	Wigglers		
	fabrication, assembly, supports, and installation	.70	
	ED&I at 15%	.10	
	Subtotal		.8
5.	Magnet Power Supplies (installed)		
	main ring	1.89	
	ED&I at 40%	.76	
	Subtotal		2.7
6.	Vacuum System Including Pumps		
	fabrication and installation	6.6	
	ED&I at 15%	1.0	
	Subtotal		7.6
7.	RF and Cryogenic System		
	Subtotal		11.5
8.	Alignment		2.0
Total Cost of Main Ring Technical Component			31.8
9.	Injector Technical Components Based on System 3		26.0
10.	Instrumentation and Controls based on 15% of technical components		8.7
11.	Conventional Facilities		
	site preparation	1.9	
	utilities	21.1	
	structures	10.9	
	cranes	.9	
	ED&I at 17.5%	6.1	
	Total Conventional Facilities		40.9
	Total Cost		107.4

VI. SUMMARY

We have described a specific design of a tau-charm factory with a luminosity of 10^{33} cm^{-2} s^{-1}. The design is based on known accelerator technology and on known collider design principles. Further general work on this design is needed in several areas.

a. A longer bunch length, σ_z, and the concomitant change in other collider parameters should be studied.

b. An injection system must be selected.

c. In the past year ideas have been presented[15] for a tau-charm factory which might attain luminosities of 5×10^{33} cm^{-2} s^{-1}. Studies should be done to see if provisions can be made in the present design for allowing upgrading to such luminosities.

ACKNOWLEDGEMENT

We wish to give our warm and heartfelt thanks to our CERN colleague, John M. Jowett, for his advice and counsel over the last two years. His initial machine design of a tau-charm factory, first published in December, 1987, had a profound effect in helping to show us the enormous physics potential experimentally accessible in the tau-charm energy region. His design formed the starting point for the machine physics investigations at the SLAC Tau-Charm Factory Workshop[3] and for the work which has lead to the Tau-Charm Factory Design presented here.

REFERENCES

1. J. Kirkby, *Proc. Int. School of Physics with Low-Energy Antiprotons, 2nd Course*, ERICE 1987, CERN-EP/87-210.
2. J. M. Jowett, CERN LEP-TH/87-56 (1987); CERN LEP-TH/88-22 (1988).
3. *Proceedings of the Tau-Charm Factory Workshop*, SLAC-REPORT-343 (1989), ed. L. Beers.
4. B. Barish *et al.*, SLAC-PUB-5053 (1989).
5. J. J. Gomez-Cadenas, C. A. Heusch, and A. Seiden, *Particle World* **1**, 10 (1989).
6. J. Kirkby, *Particle World* **1**, 27 (1989).
7. Ye Minghan, *Proceedings XIV International Symposium Lepton and Photon Interactions*, (Stanford, 1989), ed. M. Riordan.

8. K. L.Brown, T. Fieguth and J. M. Jowett, *Proceedings of the Tau-Charm Factory Workshop*, SLAC-REPORT-343 (1989), ed. L. Beers.

9. M. Donald and A. Garren, *"Vertical Separation for TCF"* in *Proceedings of the Tau-Charm Factory Workshop*, SLAC-REPORT-343 (1989), ed. L. Beers, p. 330.

10. K. A. Thompson and R. D. Ruth, I.E.E.E. Particle Accelerator Conference (1989), SLAC–PUB–4872.

11. K. A. Thompson and R. D. Ruth, SLAC–PUB–4962.

12. P. Bambade *et al.*, SLAC-PUB-4767 (1989), Phys. Rev. Lett. **62**, 2949 (1989).

13. W. Koska *et al.*, SLAC-PUB-4919 (1989), submitted to Nucl. Inst. and Meth.

14. J. C. Denard *et al.*, SLAC-PUB-4267 (1987), *Proc. IEEE Particle Accelerator Conference*, Washington, D.C. (1987) 686.

15. G. A. Voss, J. M. Paterson and S. A. Kheifets, *"Crab-Crossing in a Tau-Charm Facility"* in *Proceedings of the Tau-Charm Factory Workshop*, SLAC-REPORT-343 (1989), ed. L. Beers, p.31. Also SLAC-PUB-5011 (1989).

FIGURE CAPTIONS

1. Schematic of the tau-charm factory. In this design a linac is used after the accumulator/damping ring in the injector; an alternative design would use a booster synchrotron. Injection system #3 (Sec. III.D) is pictured.
2. Main energy range of a tau-charm factory.
3. The luminosity of present and future electron-positron colliders.
4. Cell structure and magnets in a half ring.
5. $\sqrt{B_x}$ and $\sqrt{B_y}$ vs. s for half ring.
6. Beam envelope in terms of $10\,\sigma_x$ and $10\,\sigma_y$ vs. s for half ring. Note: the 10° and 20° cells shown are typical cells, hence the discontinuities in $10\,\sigma_x$.
7. Luminosity versus beam energy when the maximum is set at 2.2 GeV.
8. Schematic of the interaction region (IR).
9. Schematic of the insertion system leading to the IR.
10. A 20° and a 10° cell.
11. Schematic of the magnet support system in a 20° cell.
12. Longitudinal and transverse growth rates as a function of Q-reduction factor. In Figs. 12a, b, and c, maximum longitudinal growth rates are shown, assuming 0%, 0.1% and 1.0% total cell-to-cell spread in RF cavity mode frequencies, respectively. In Fig. 12d, maximum transverse growth rates are shown, for the case of 1.0% frequency spread. The points labelled H are those for the high-frequency RF system (1500 MHz), and the points labelled L are those for the low-frequency RF system (350 MHz).
13. Summary of four alternate injection system designs.
14. The collider housing.
15. The injector housing.
16. Side view of collider hall.
17. Top view of collider hall.

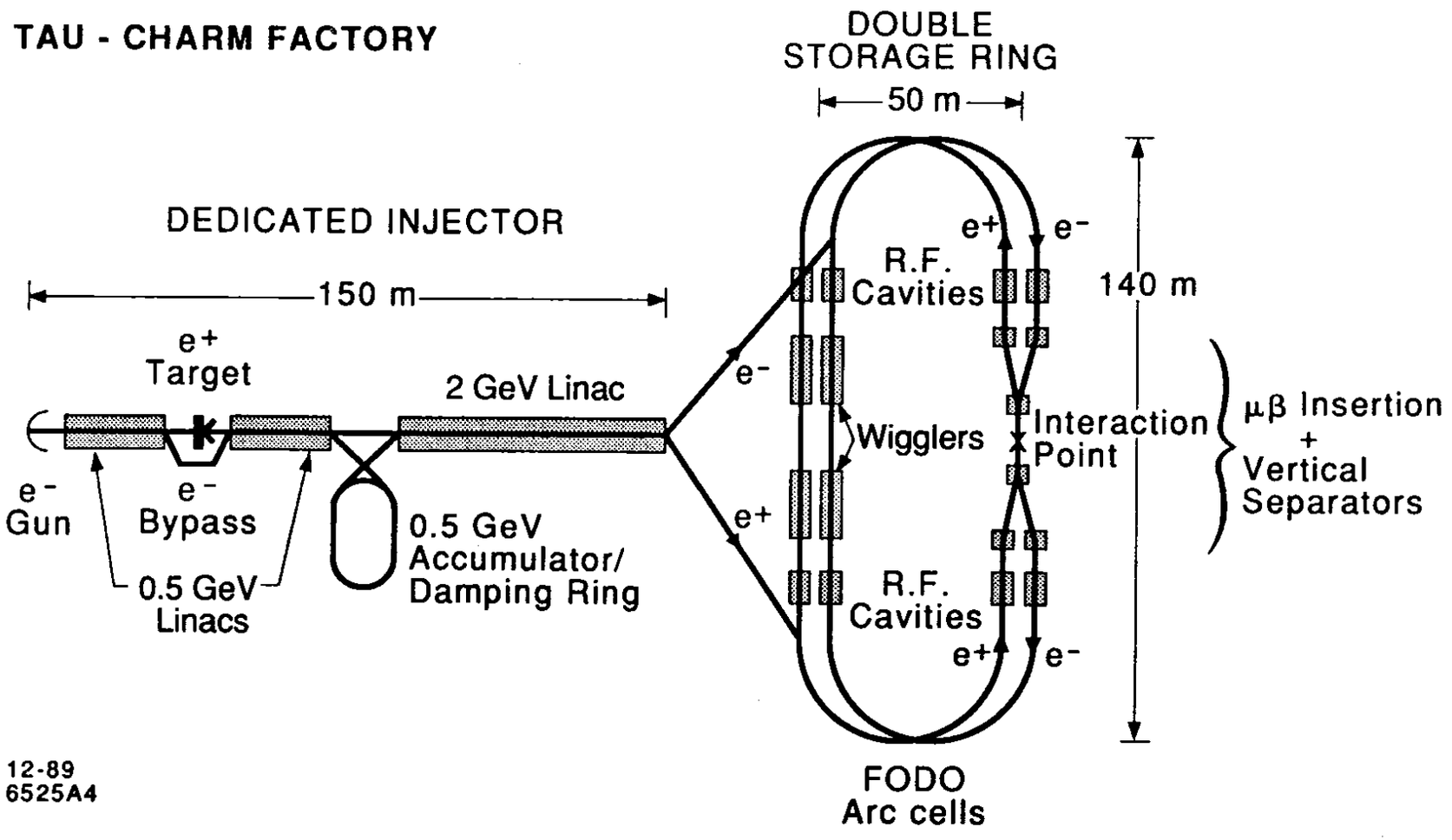
TAU - CHARM FACTORY
DOUBLE
STORAGE RING
50 m
DEDICATED INJECTOR
150 m
e+
Target
2 GeV Linac
e-
Gun
e-
Bypass
0.5 GeV
Linacs
0.5 GeV
Accumulator/
Damping Ring
e+
e-
R.F.
Cavities
Wigglers
Interaction
Point
R.F.
Cavities
e+
e-
e+
e-
140 m
μβ Insertion
+
Vertical
Separators
FODO
Arc cells
12-89
6525A4

Figure 1

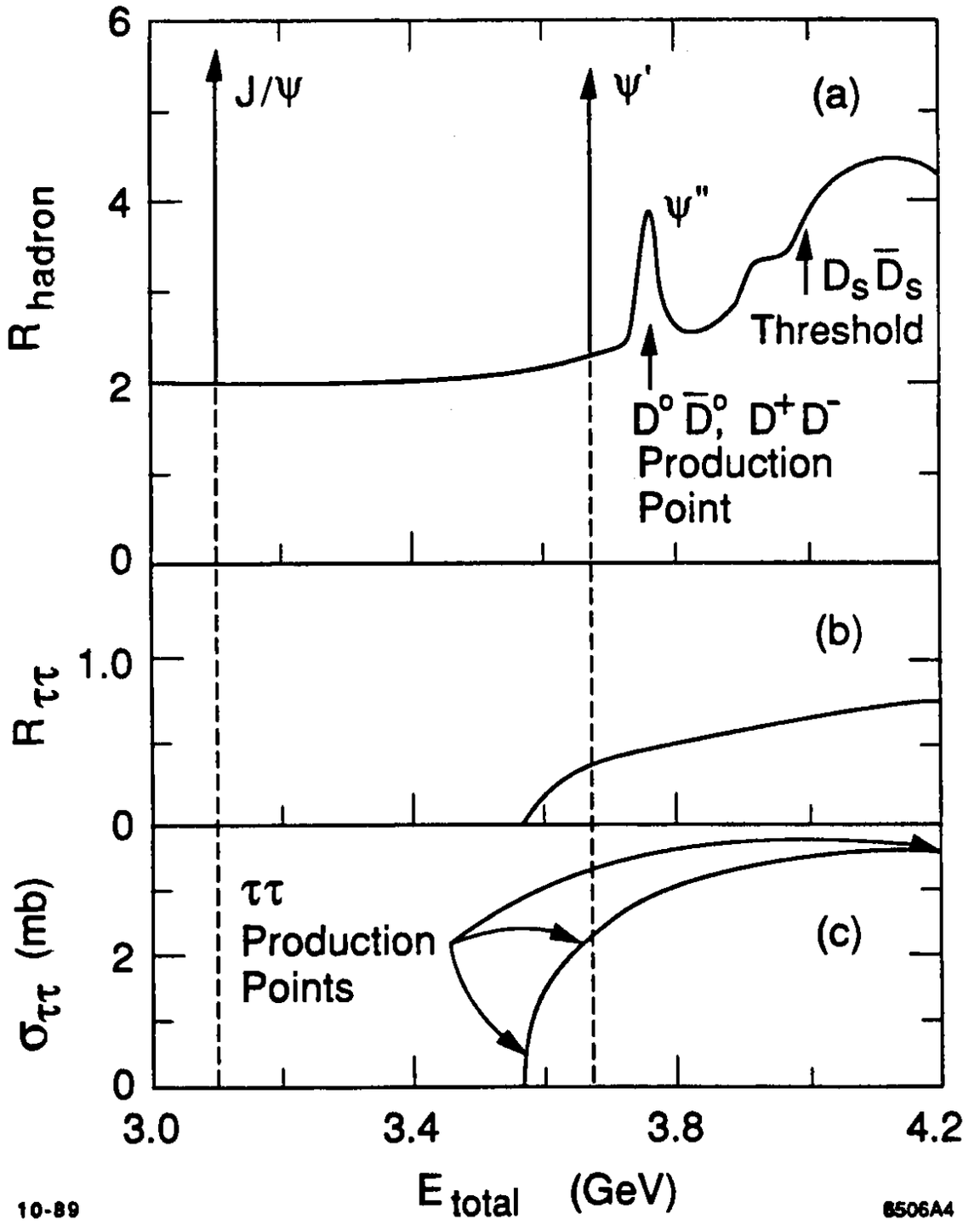
6
4
2
0
J/ψ
ψ'
(a)
ψ"
$D_s \bar{D}_s$
Threshold
$D^0 \bar{D}^0$, $D^+ D^-$
Production
Point
R_{hadron}
1.0
0
(b)
$R_{\tau\tau}$
2
0
ττ
Production
Points
(c)
$\sigma_{\tau\tau}$ (mb)
3.0
3.4
3.8
4.2
E_{total} (GeV)
10-89
8506A4

Figure 2

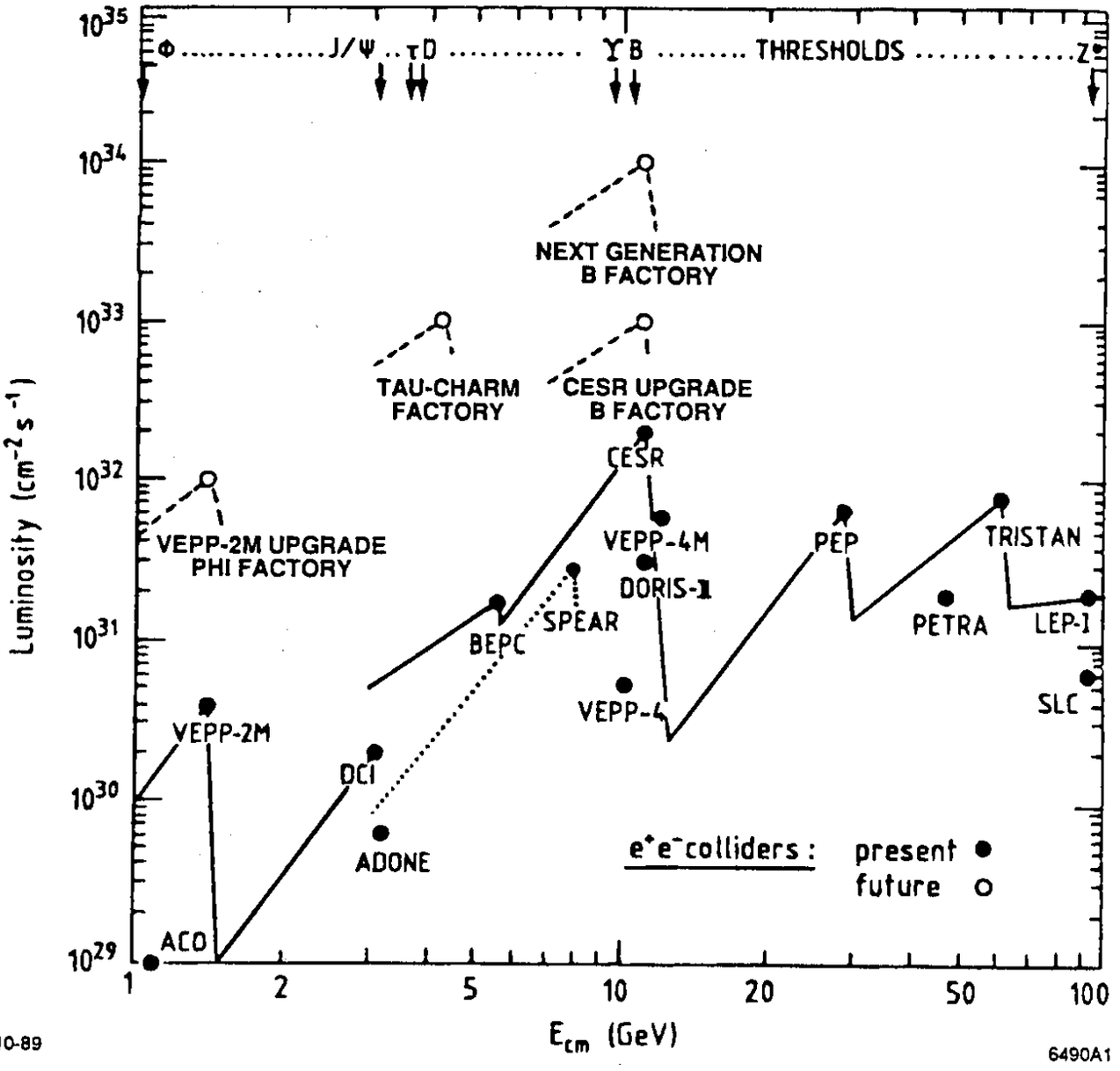
Φ ..... J/Ψ .. τD ..... ϒB ..... THRESHOLDS ..... Z
NEXT GENERATION B FACTORY
TAU-CHARM FACTORY
CESR UPGRADE B FACTORY
CESR
VEPP-2M UPGRADE PHI FACTORY
VEPP-4M
DORIS-1
PEP
TRISTAN
SPEAR
BEPC
PETRA
LEP-I
VEPP-4
SLC
VEPP-2M
DCI
ADONE
ACO
e⁺e⁻colliders : present ●
future ○
Luminosity (cm⁻² s⁻¹)
E_cm (GeV)
10-89
6490A1

Figure 3

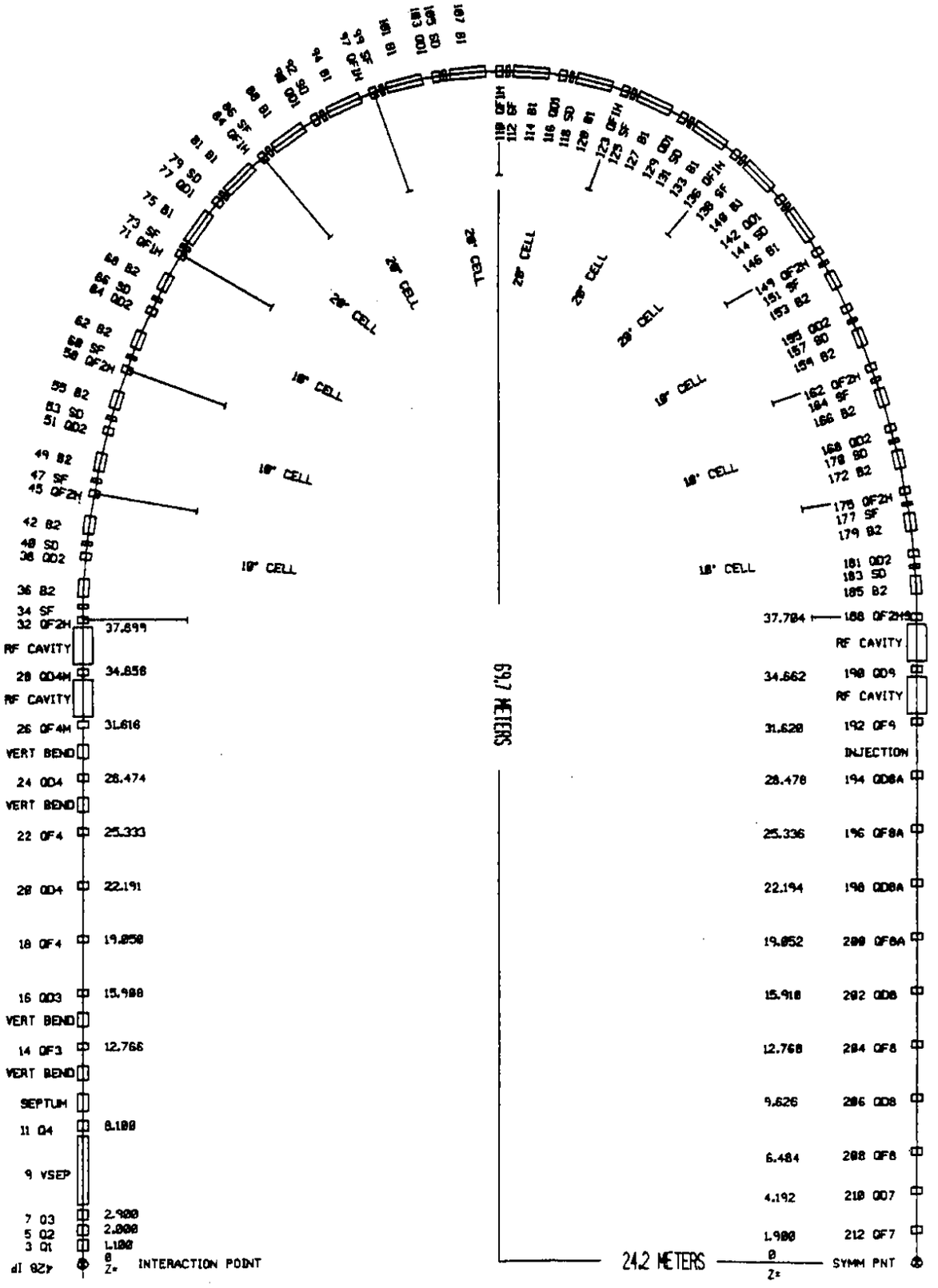
69.7 METERS
24.2 METERS
INTERACTION POINT
SYMM PNT
RF CAVITY
VERT BEND
SEPTUM
INJECTION
18° CELL
20° CELL

Figure 4

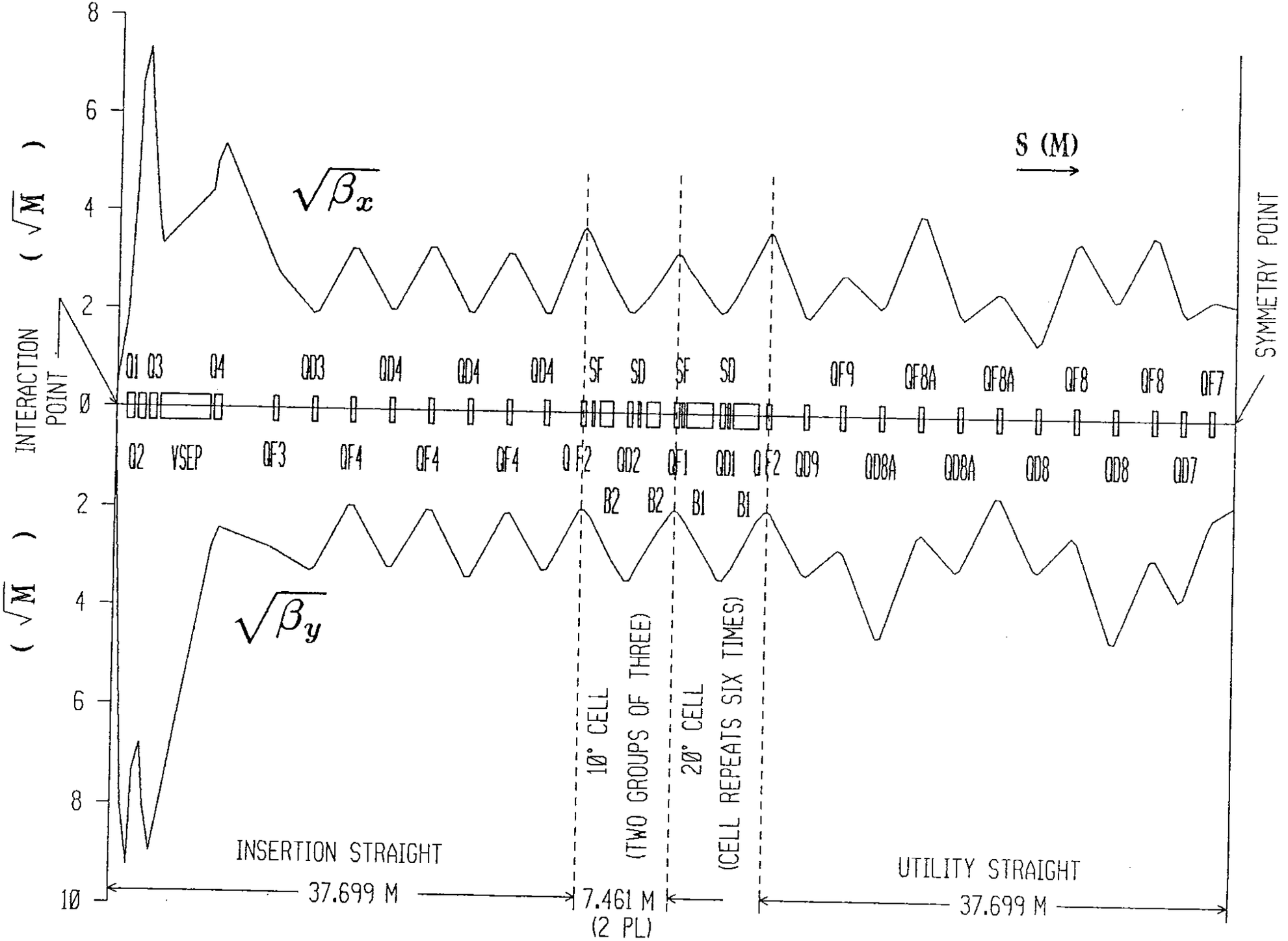
8
6
4
2
Ø
2
4
6
8
10
(√M)
(√M)
INTERACTION POINT
S (M)
SYMMETRY POINT
√βx
√βy
Q1 Q3 Q4 QD3 QD4 QD4 QD4 SF SD SF SD QF9 QF8A QF8A QF8 QF8 QF7
Q2 VSEP QF3 QF4 QF4 QF4 QF2 QD2 QF1 QD1 QF2 QD9 QD8A QD8A QD8 QD8 QD7
B2 B2 B1 B1
10° CELL
(TWO GROUPS OF THREE)
20° CELL
(CELL REPEATS SIX TIMES)
INSERTION STRAIGHT
37.699 M
7.461 M
(2 PL)
UTILITY STRAIGHT
37.699 M

Figure 5

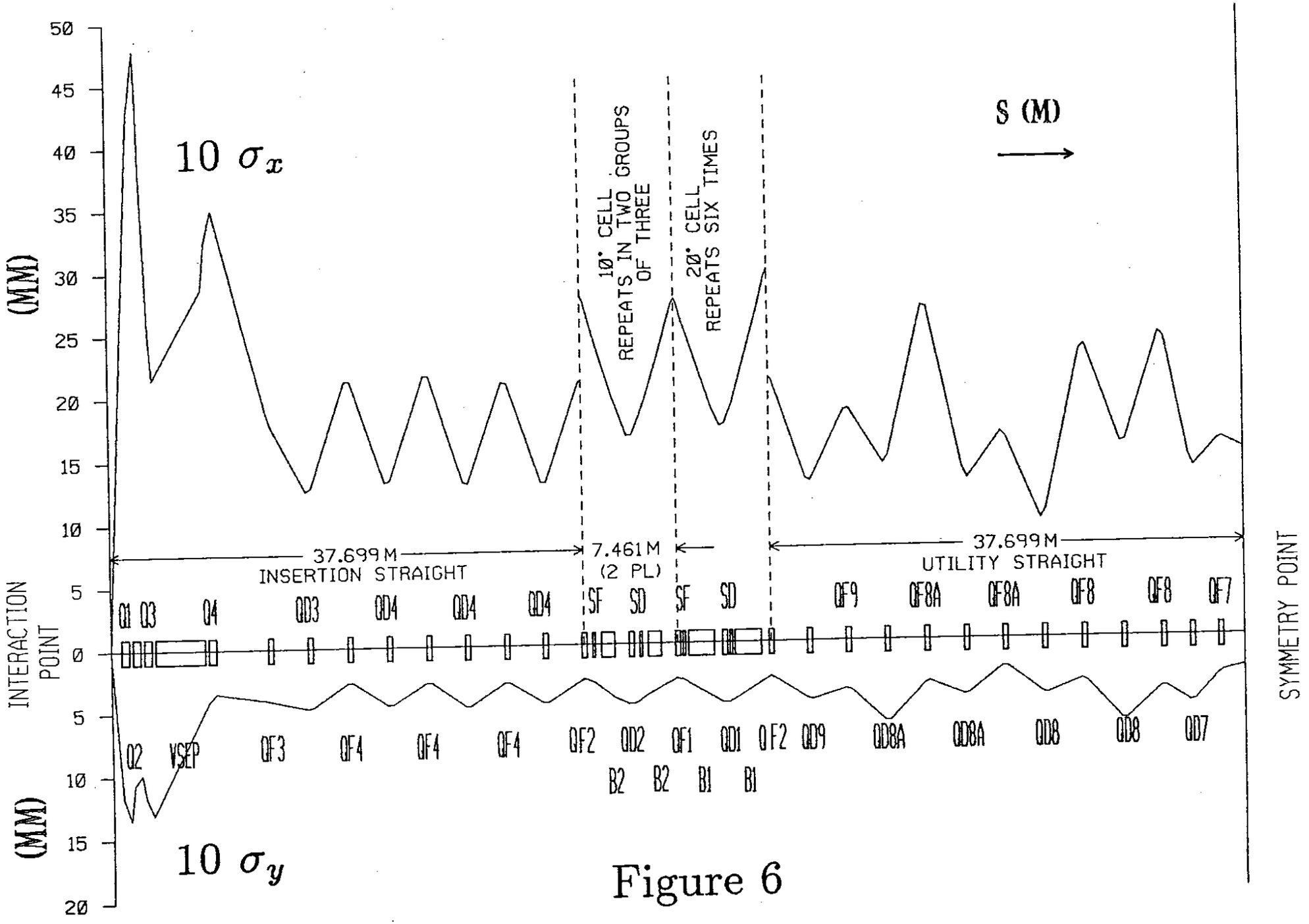
50
45
40
35
30
25
20
15
10
5
0
5
10
15
20
(MM)
10 σ_x
10 σ_y
S (M)
10° CELL
REPEATS IN TWO
OF THREE GROUPS
20° CELL
REPEATS SIX TIMES
37.699 M
INSERTION STRAIGHT
7.461 M
(2 PL)
37.699 M
UTILITY STRAIGHT
INTERACTION
POINT
SYMMETRY POINT
Q1 Q3 Q4 QD3 QD4 QD4 QD4 SF SD SF SD QF9 QF8A QF8A QF8 QF8 QF7
Q2 VSEP QF3 QF4 QF4 QF4 QF2 QD2 QF1 QD1 QF2 QD9 QD8A QD8A QD8 QD8 QD7
B2 B2 B1 B1

Figure 6

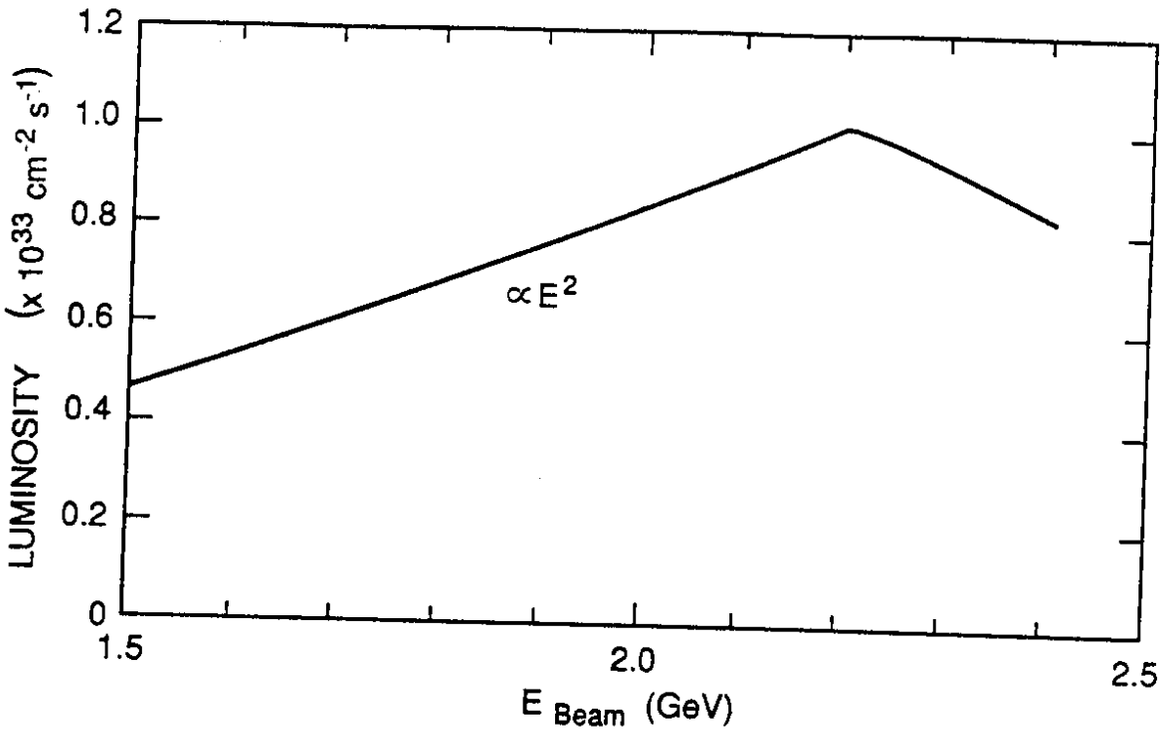

Figure 7

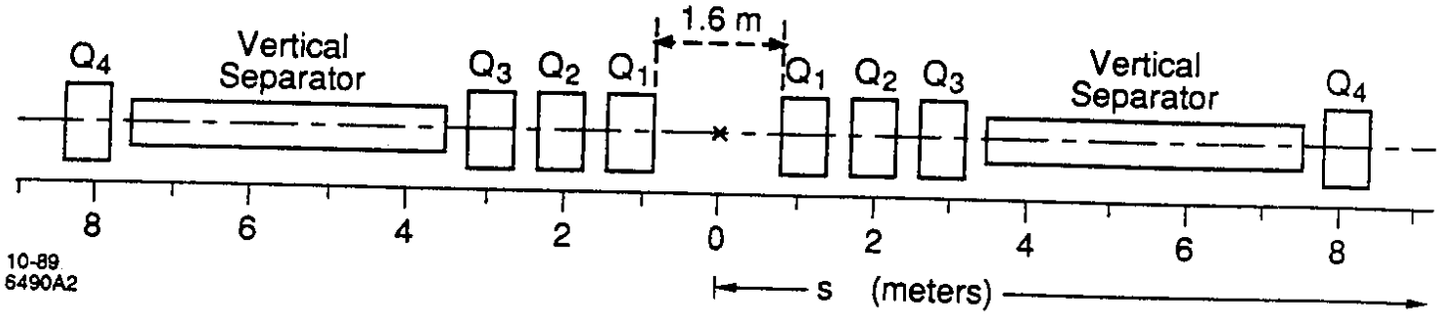

Figure 8

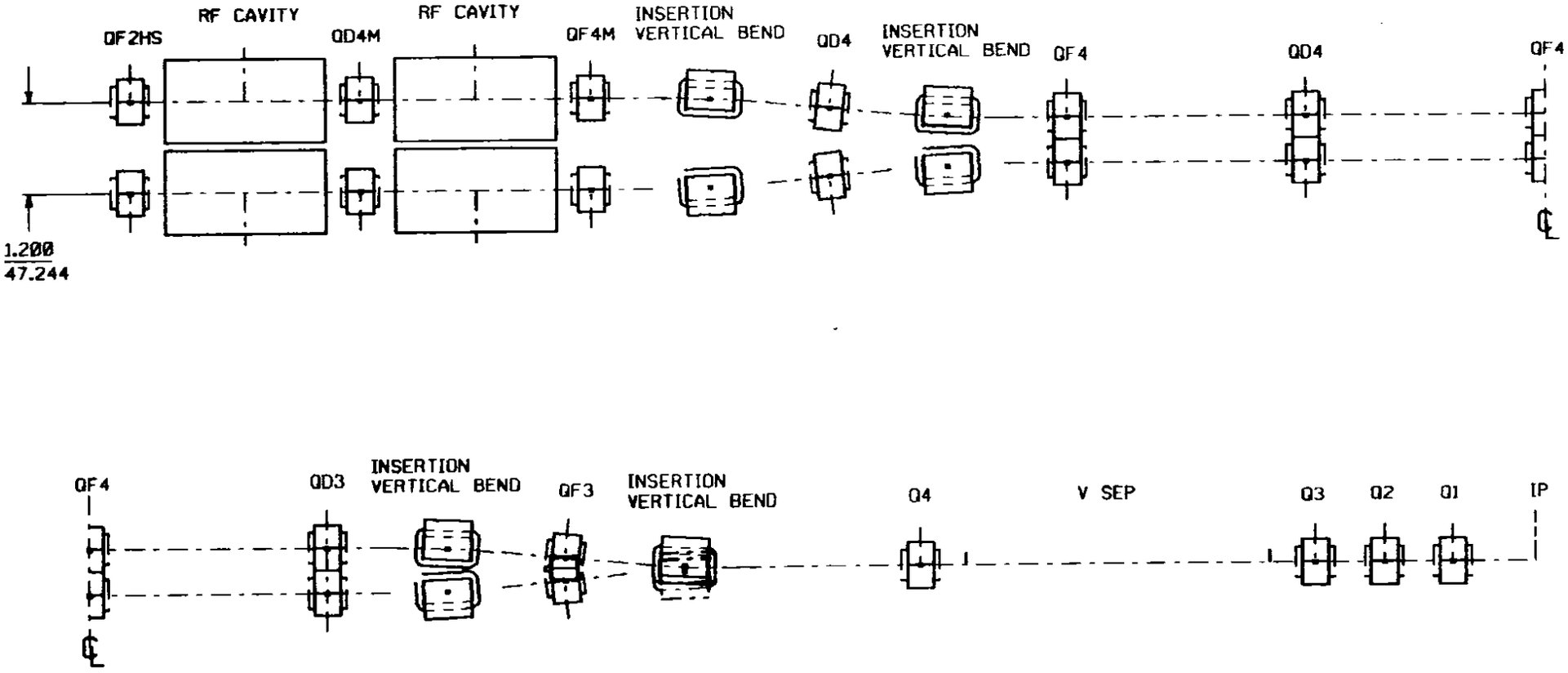

INSERTION STRAIGHT ELEVATION

Figure 9

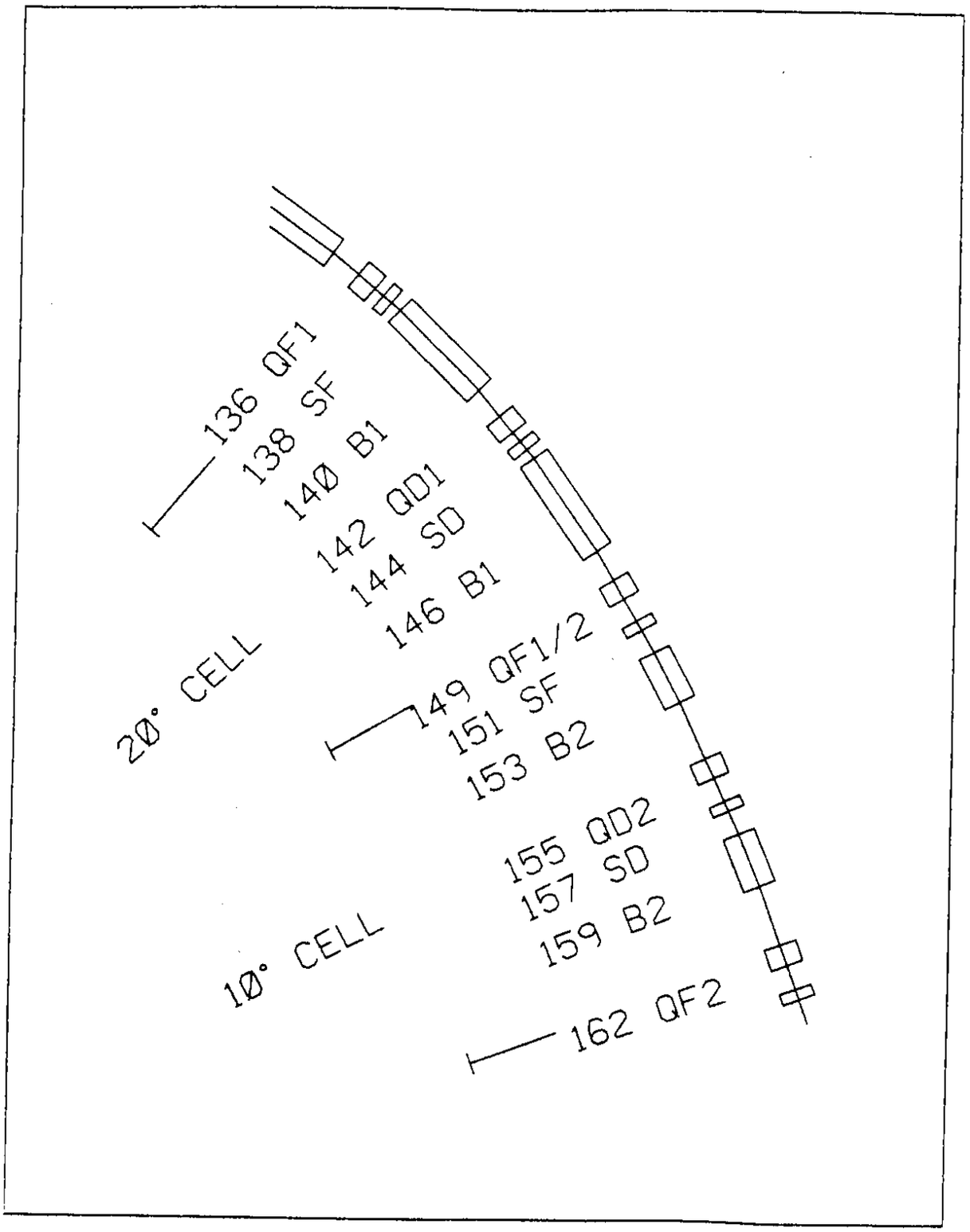
136 QF1
138 SF
140 B1
142 QD1
144 SD
146 B1
20° CELL
149 QF1/2
151 SF
153 B2
155 QD2
157 SD
159 B2
10° CELL
162 QF2

Figure 10

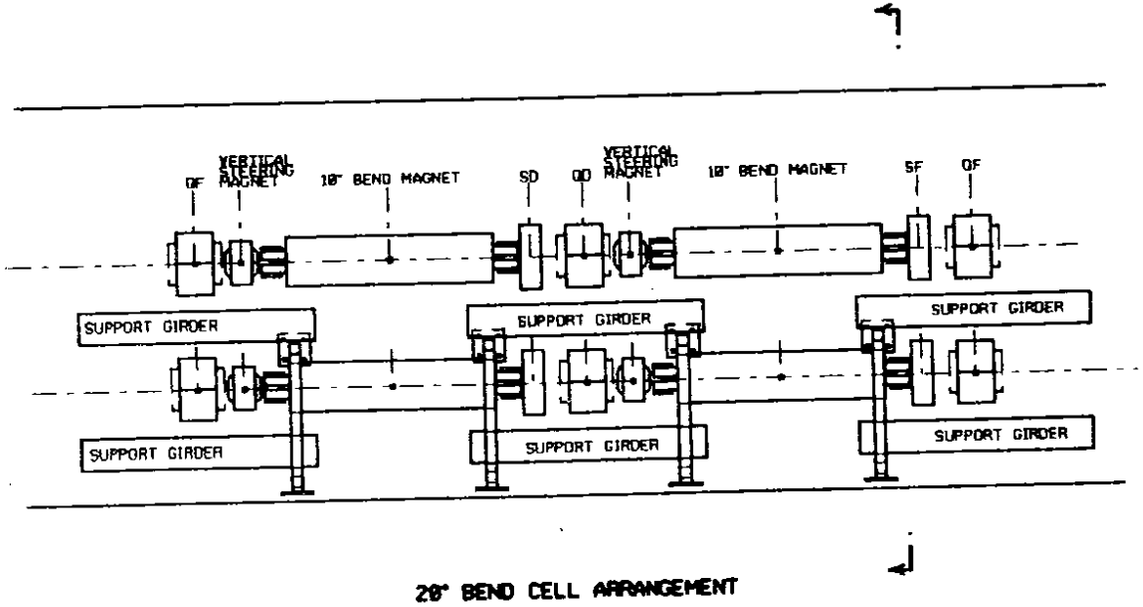
QF
VERTICAL STEERING MAGNET
18° BEND MAGNET
SD
QD
VERTICAL STEERING MAGNET
18° BEND MAGNET
SF
QF
SUPPORT GIRDER
SUPPORT GIRDER
SUPPORT GIRDER
SUPPORT GIRDER
SUPPORT GIRDER
20° BEND CELL ARRANGEMENT

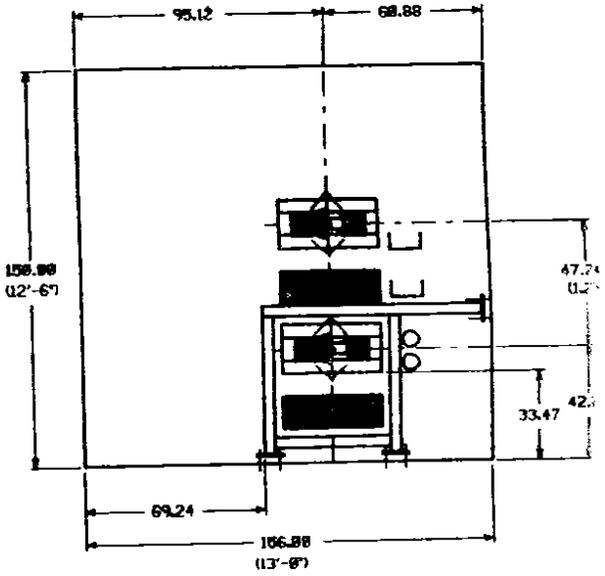
95.12
68.88
158.88
(12'-6")
33.47
69.24
166.88
(13'-6")

Figure 11

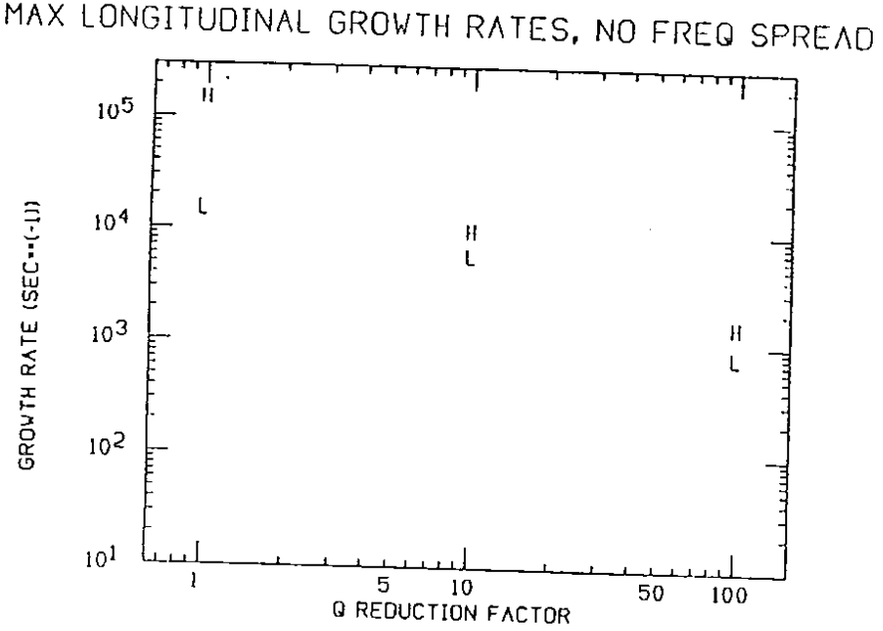

Fig. 12a

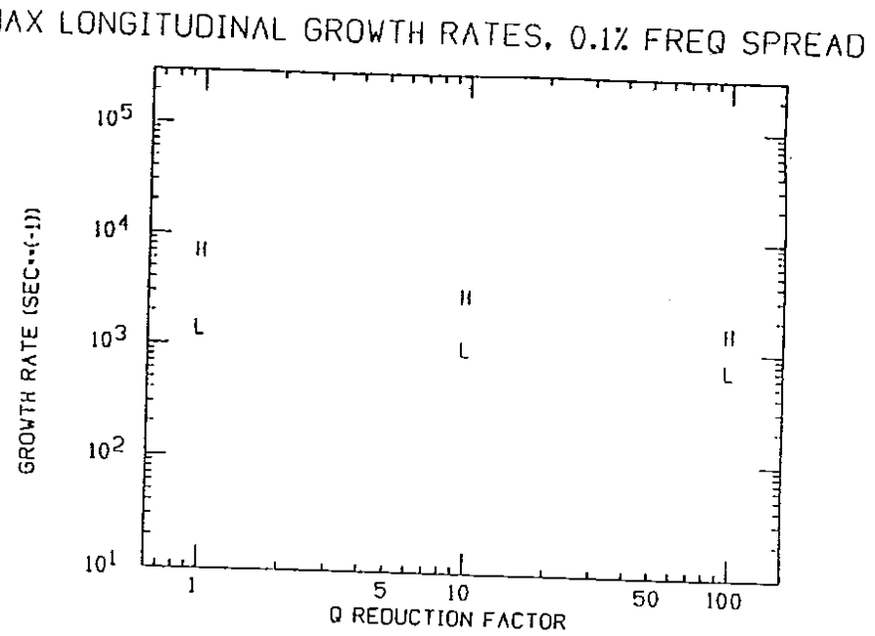

Fig. 12b

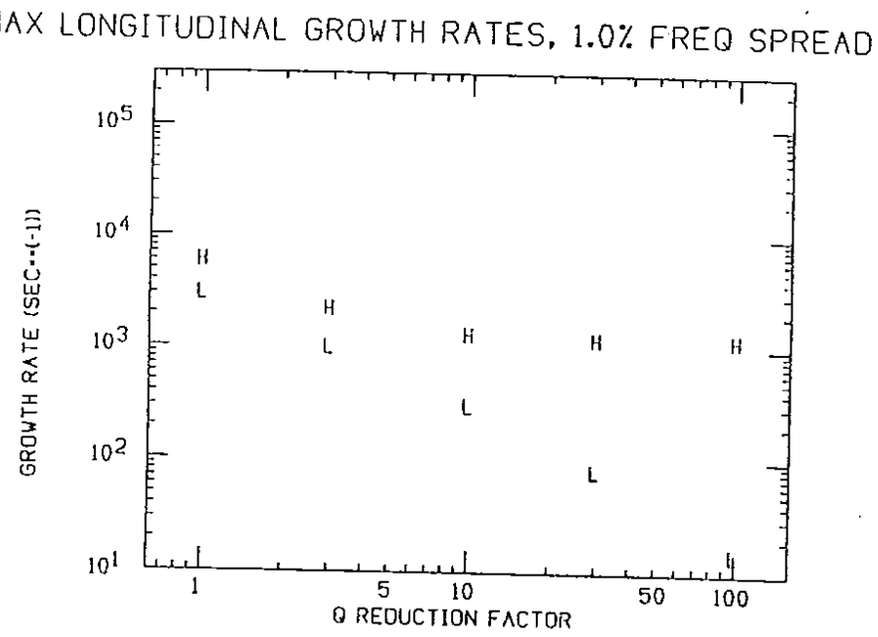

Fig. 12c

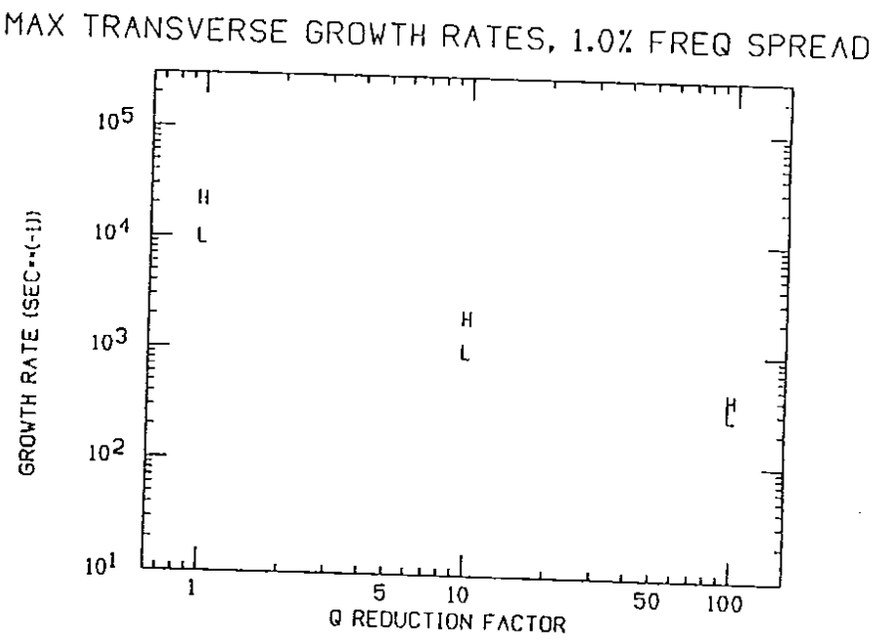

Fig. 12d

Figure 12

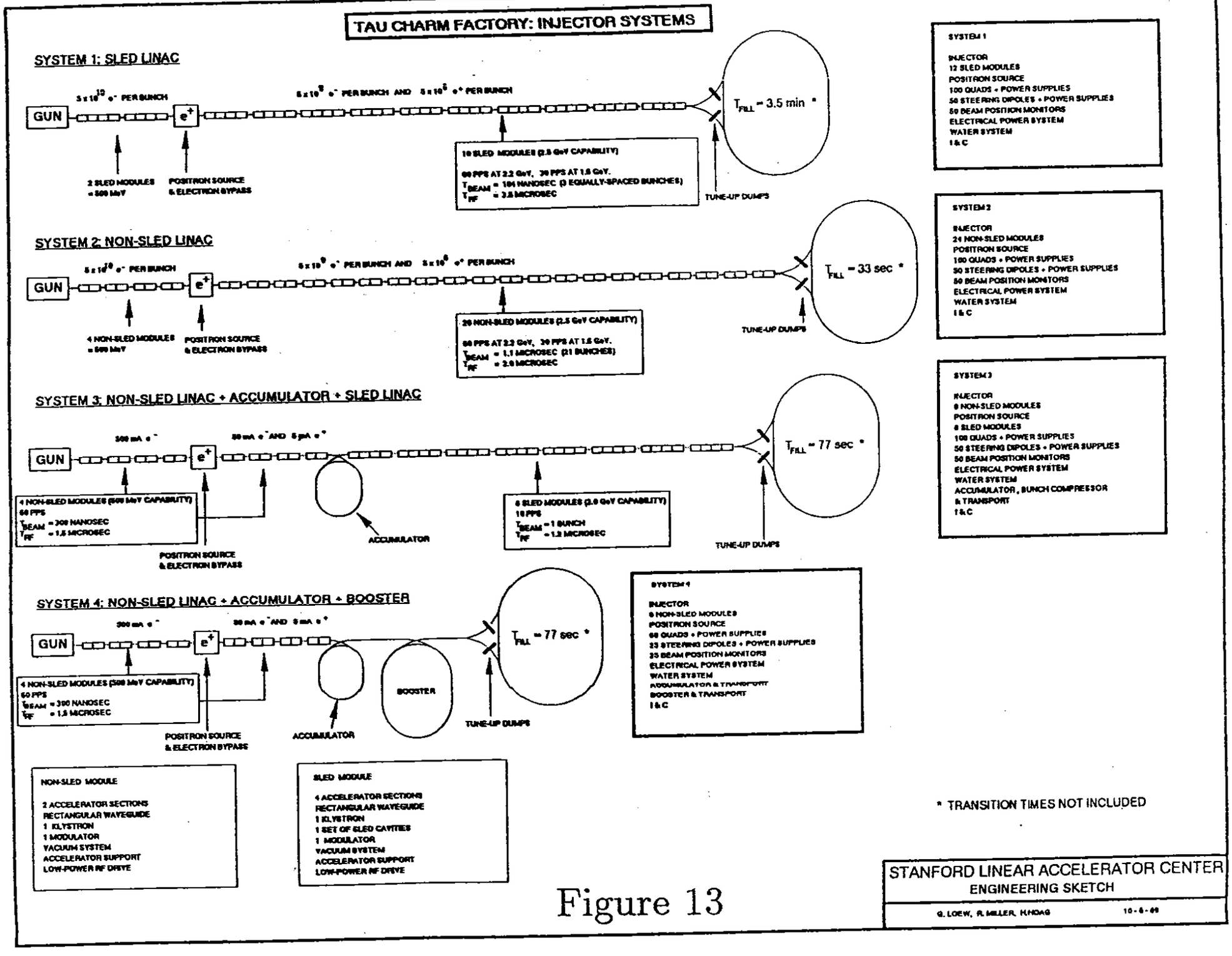
TAU CHARM FACTORY: INJECTOR SYSTEMS
SYSTEM 1: SLED LINAC
GUN
e+
2 SLED MODULES
POSITRON SOURCE
& ELECTRON BYPASS
10 SLED MODULES (2.5 GeV CAPABILITY)
60 PPS AT 2.2 GeV, 30 PPS AT 1.5 GeV.
T_BEAM = 154 NANOSEC (3 EQUALLY-SPACED BUNCHES)
T_RF = 3.5 MICROSEC
T_FILL = 3.5 min *
TUNE-UP DUMPS
SYSTEM 1
INJECTOR
12 SLED MODULES
POSITRON SOURCE
100 QUADS + POWER SUPPLIES
50 STEERING DIPOLES + POWER SUPPLIES
50 BEAM POSITION MONITORS
ELECTRICAL POWER SYSTEM
WATER SYSTEM
I & C
SYSTEM 2: NON-SLED LINAC
GUN
e+
4 NON-SLED MODULES
POSITRON SOURCE
& ELECTRON BYPASS
20 NON-SLED MODULES (2.5 GeV CAPABILITY)
60 PPS AT 2.2 GeV, 30 PPS AT 1.5 GeV.
T_BEAM = 1.1 MICROSEC (21 BUNCHES)
T_RF = 2.8 MICROSEC
T_FILL = 33 sec *
TUNE-UP DUMPS
SYSTEM 2
INJECTOR
24 NON-SLED MODULES
POSITRON SOURCE
100 QUADS + POWER SUPPLIES
50 STEERING DIPOLES + POWER SUPPLIES
50 BEAM POSITION MONITORS
ELECTRICAL POWER SYSTEM
WATER SYSTEM
I & C
SYSTEM 3: NON-SLED LINAC + ACCUMULATOR + SLED LINAC
GUN
e+
4 NON-SLED MODULES (500 MeV CAPABILITY)
60 PPS
T_BEAM = 300 NANOSEC
T_RF = 1.5 MICROSEC
POSITRON SOURCE
& ELECTRON BYPASS
ACCUMULATOR
6 SLED MODULES (2.0 GeV CAPABILITY)
10 PPS
T_BEAM = 1 BUNCH
T_RF = 1.2 MICROSEC
T_FILL = 77 sec *
TUNE-UP DUMPS
SYSTEM 3
INJECTOR
8 NON-SLED MODULES
POSITRON SOURCE
6 SLED MODULES
100 QUADS + POWER SUPPLIES
50 STEERING DIPOLES + POWER SUPPLIES
50 BEAM POSITION MONITORS
ELECTRICAL POWER SYSTEM
WATER SYSTEM
ACCUMULATOR, BUNCH COMPRESSOR
& TRANSPORT
I & C
SYSTEM 4: NON-SLED LINAC + ACCUMULATOR + BOOSTER
GUN
e+
4 NON-SLED MODULES (500 MeV CAPABILITY)
60 PPS
T_BEAM = 300 NANOSEC
T_RF = 1.5 MICROSEC
POSITRON SOURCE
& ELECTRON BYPASS
ACCUMULATOR
BOOSTER
TUNE-UP DUMPS
T_FILL = 77 sec *
SYSTEM 4
INJECTOR
6 NON-SLED MODULES
POSITRON SOURCE
68 QUADS + POWER SUPPLIES
23 STEERING DIPOLES + POWER SUPPLIES
23 BEAM POSITION MONITORS
ELECTRICAL POWER SYSTEM
WATER SYSTEM
ACCUMULATOR & TRANSPORT
BOOSTER & TRANSPORT
I & C
NON-SLED MODULE
2 ACCELERATOR SECTIONS
RECTANGULAR WAVEGUIDE
1 KLYSTRON
1 MODULATOR
VACUUM SYSTEM
ACCELERATOR SUPPORT
LOW-POWER RF DRIVE
SLED MODULE
4 ACCELERATOR SECTIONS
RECTANGULAR WAVEGUIDE
1 KLYSTRON
1 SET OF SLED CAVITIES
1 MODULATOR
VACUUM SYSTEM
ACCELERATOR SUPPORT
LOW-POWER RF DRIVE
* TRANSITION TIMES NOT INCLUDED
STANFORD LINEAR ACCELERATOR CENTER
ENGINEERING SKETCH
G. LOEW, R. MILLER, H.HOAG
10-6-88

Figure 13

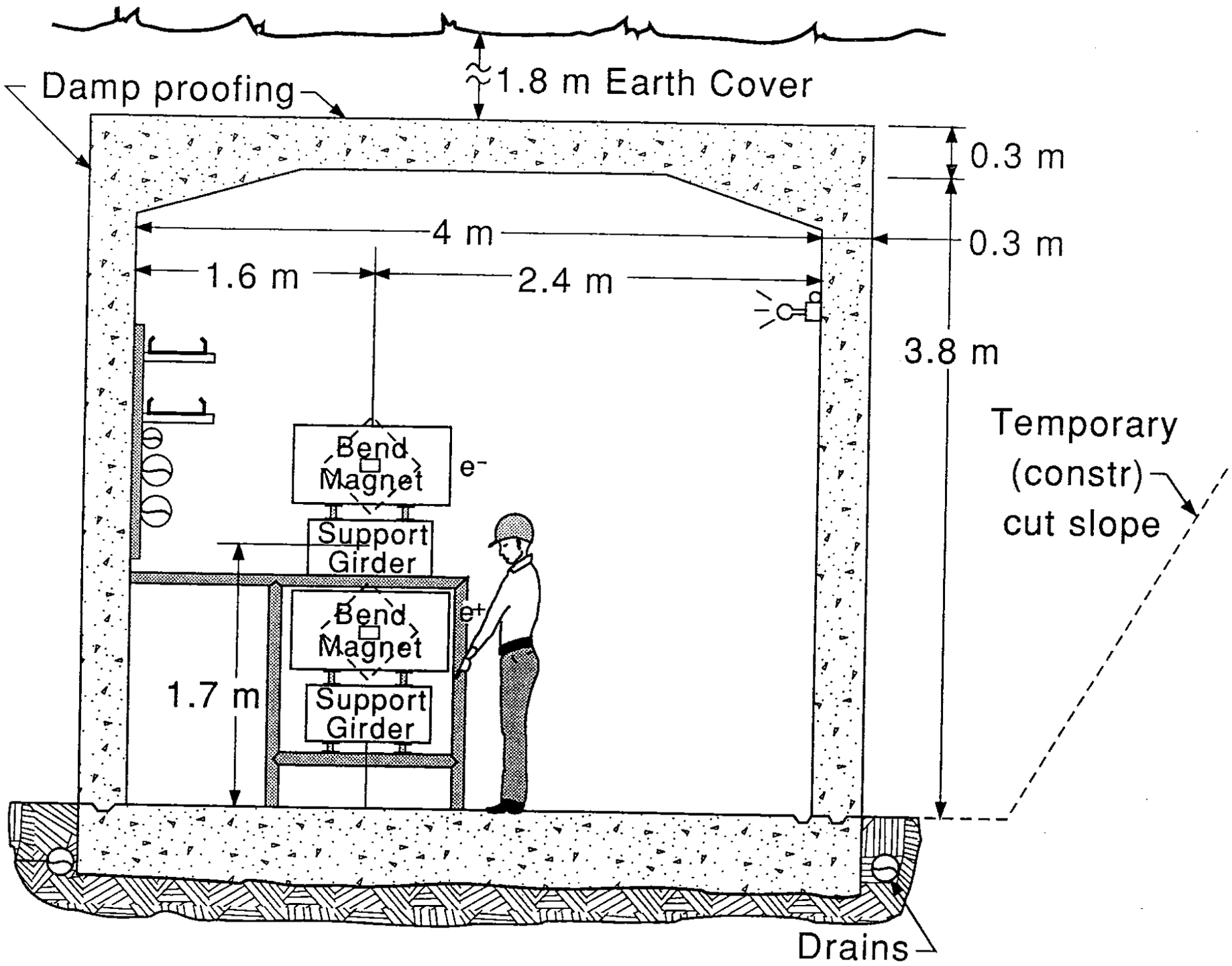

12-89

Figure 14

6525A1

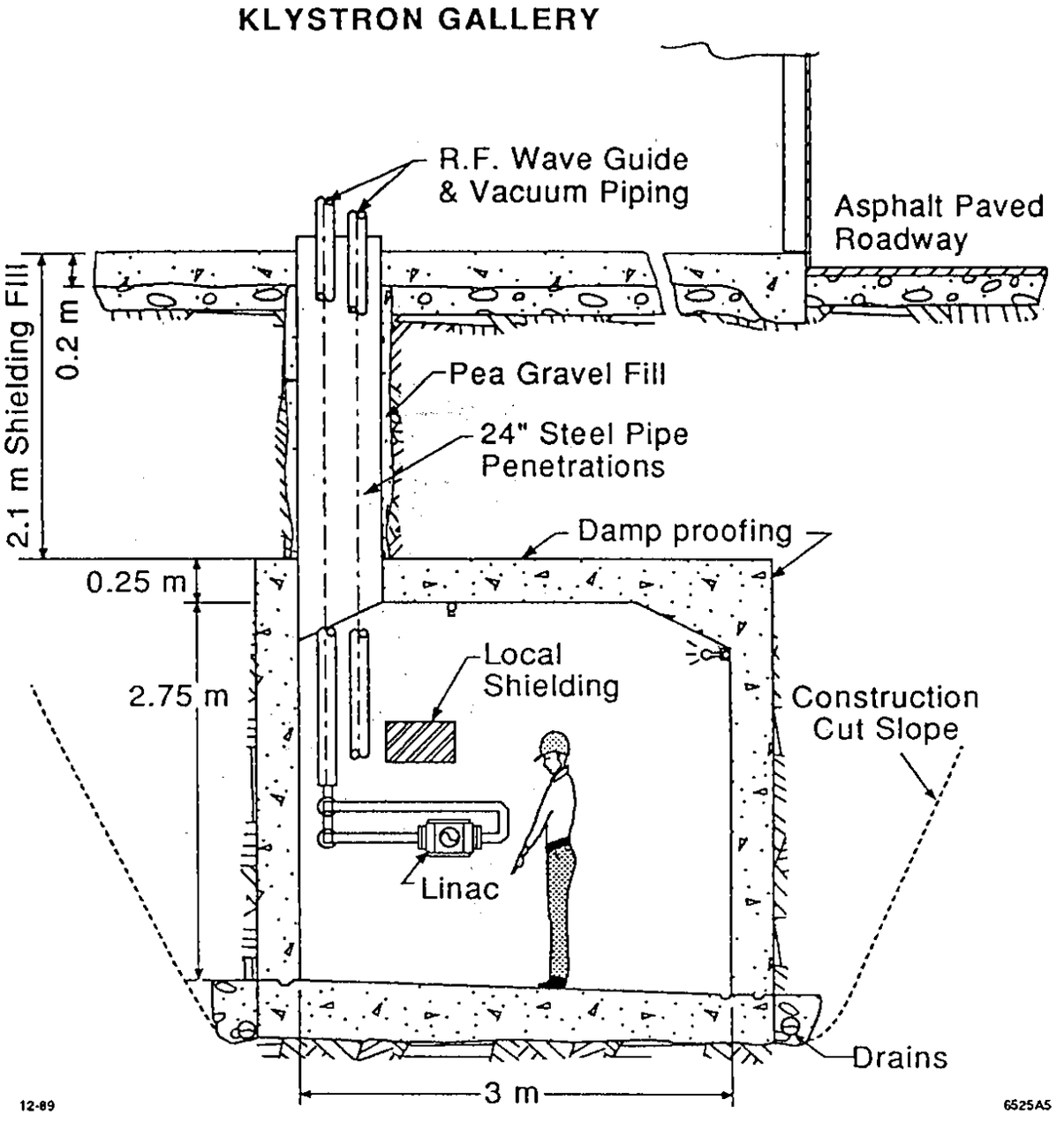
KLYSTRON GALLERY
R.F. Wave Guide
& Vacuum Piping
Asphalt Paved
Roadway
2.1 m Shielding Fill
0.2 m
Pea Gravel Fill
24" Steel Pipe
Penetrations
Damp proofing
0.25 m
2.75 m
Local
Shielding
Construction
Cut Slope
Linac
Drains
3 m
12-89
6525A5

Figure 15

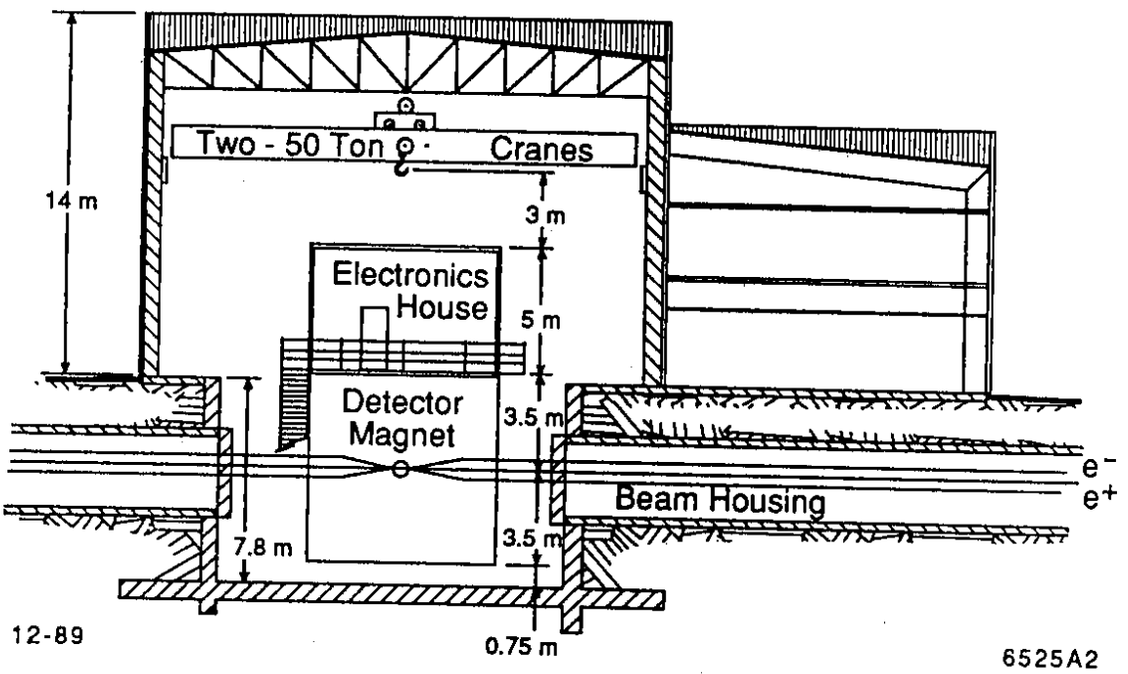
Two - 50 Ton Cranes
14 m
3 m
Electronics House
5 m
Detector Magnet
3.5 m
e⁻
e⁺
Beam Housing
7.8 m
3.5 m
0.75 m
12-89
6525A2

Figure 16

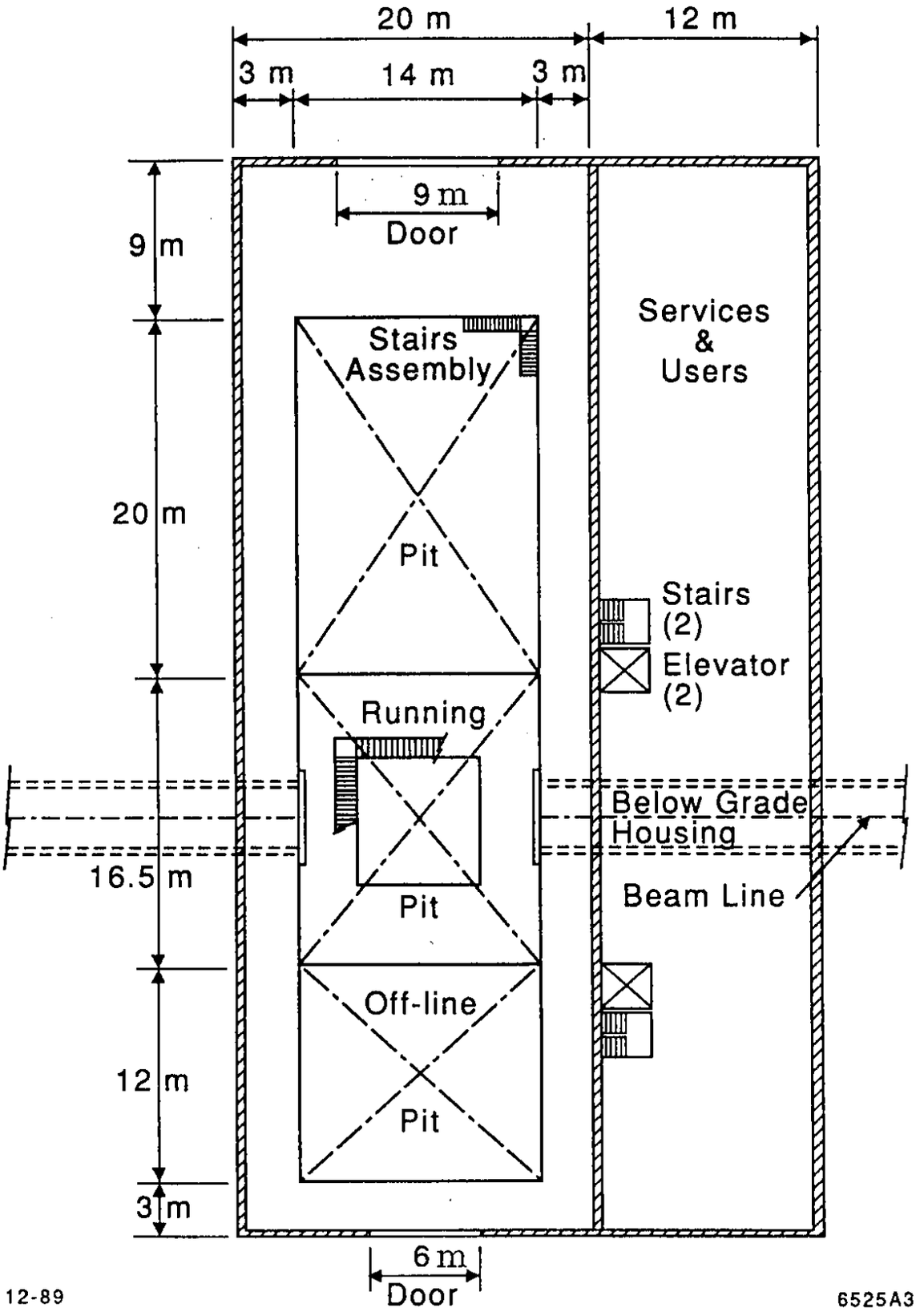
20 m
12 m
3 m
14 m
3 m
9 m
Door
9 m
Services
&
Users
Stairs
Assembly
20 m
Pit
Stairs
(2)
Elevator
(2)
Running
Below Grade
Housing
16.5 m
Pit
Beam Line
Off-line
12 m
Pit
3 m
6 m
Door
12-89
6525A3

Figure 17